Hindawi Publishing Corporation
International Journal of Chemical Engineering
Volume 2012, Article ID 759397, 31 pages
doi:10.1155/2012/759397

Review Article

CFD Simulation of Annular Centrifugal Extractors

S. Vedantam,[1] K. E. Wardle,[2] T. V. Tamhane,[3] V. V. Ranade,[1] and J. B. Joshi[3,4]

[1] *Chemical Engineering and Process Development Division, National Chemical Laboratory, Pune 411008, India*
[2] *Chemical Sciences and Engineering Division, Argonne National Laboratory, Lemont, IL 60439, USA*
[3] *Department of Chemical Engineering, Institute of Chemical Technology, Matunga, Mumbai 400 019, India*
[4] *Homi Bhabha National Institute, Anushakti Nagar, Mumbai 400 094, India*

Correspondence should be addressed to K. E. Wardle, kwardle@anl.gov and J. B. Joshi, jbjoshi@gmail.com

Received 30 March 2012; Accepted 13 June 2012

Academic Editor: Mahesh T. Dhotre

Copyright © 2012 S. Vedantam et al. This is an open access article distributed under the Creative Commons Attribution License, which permits unrestricted use, distribution, and reproduction in any medium, provided the original work is properly cited.

Annular centrifugal extractors (ACE), also called annular centrifugal contactors offer several advantages over the other conventional process equipment such as low hold-up, high process throughput, low residence time, low solvent inventory and high turn down ratio. The equipment provides a very high value of mass transfer coefficient and interfacial area in the annular zone because of the high level of power consumption per unit volume and separation inside the rotor due to the high g of centrifugal field. For the development of rational and reliable design procedures, it is important to understand the flow patterns in the mixer and settler zones. Computational Fluid Dynamics (CFD) has played a major role in the constant evolution and improvements of this device. During the past thirty years, a large number of investigators have undertaken CFD simulations. All these publications have been carefully and critically analyzed and a coherent picture of the present status has been presented in this review paper. Initially, review of the single phase studies in the annular region has been presented, followed by the separator region. In continuation, the two-phase CFD simulations involving liquid-liquid and gas-liquid flow in the annular as well as separator regions have been reviewed. Suggestions have been made for the future work for bridging the existing knowledge gaps. In particular, emphasis has been given to the application of CFD simulations for the design of this equipment.

1. Introduction

Annular centrifugal extractors, also called annular centrifugal contactors [1–5], offer several advantages over the other conventional process equipment such as low holdup, high process throughput, low residence time, low solvent inventory, and high turndown ratio. The equipment provides a very high value of mass transfer coefficient and interfacial area in the annular zone because of the high level of power consumption per unit volume [6, 7] and separation inside the rotor due to the high g of centrifugal field. Annular centrifugal extractors find wide applications in nuclear fuel processing where safety is the main concern [2, 8, 9], in biological operations where controlled shear field and/or facilitated settling is important [10, 11] and polymerization [12, 13], excellent mixing, heat, and mass transfer [14–19]. Annular centrifugal extractors can also be used for a variety of chemical reactions such as synthesis of monodisperse silica particles, regeneration of spent activated carbon [20, 21], esterification, and hydrolysis [22, 23], as cavitation reactor [24], and they have also been demonstrated for use with ionic liquids [25].

Depending upon the orientation of rotating cylinder, the equipment is classified as a horizontal or vertical contactor. In both types of contactors, the flow behavior can be broadly classified as either a homogeneous dispersion, banded dispersion, or stratified flow with both the phases retaining their individual integrity. To design this equipment, it is important to understand a priori the conditions under which the transition takes place from one type of flow regime to another. Industrial scale equipment typically has a vertical orientation [26–28]. Some published work is also available for horizontal orientation [4, 29, 30].

The annular centrifugal extractor (ACE) consists of coaxial cylinders ((1) and (2)) as shown schematically in Figure 1. The immiscible feed liquids enter at points (3A) and (3B) into the annular region between the two cylinders. The spinning of the rotor imparts power (in the range of

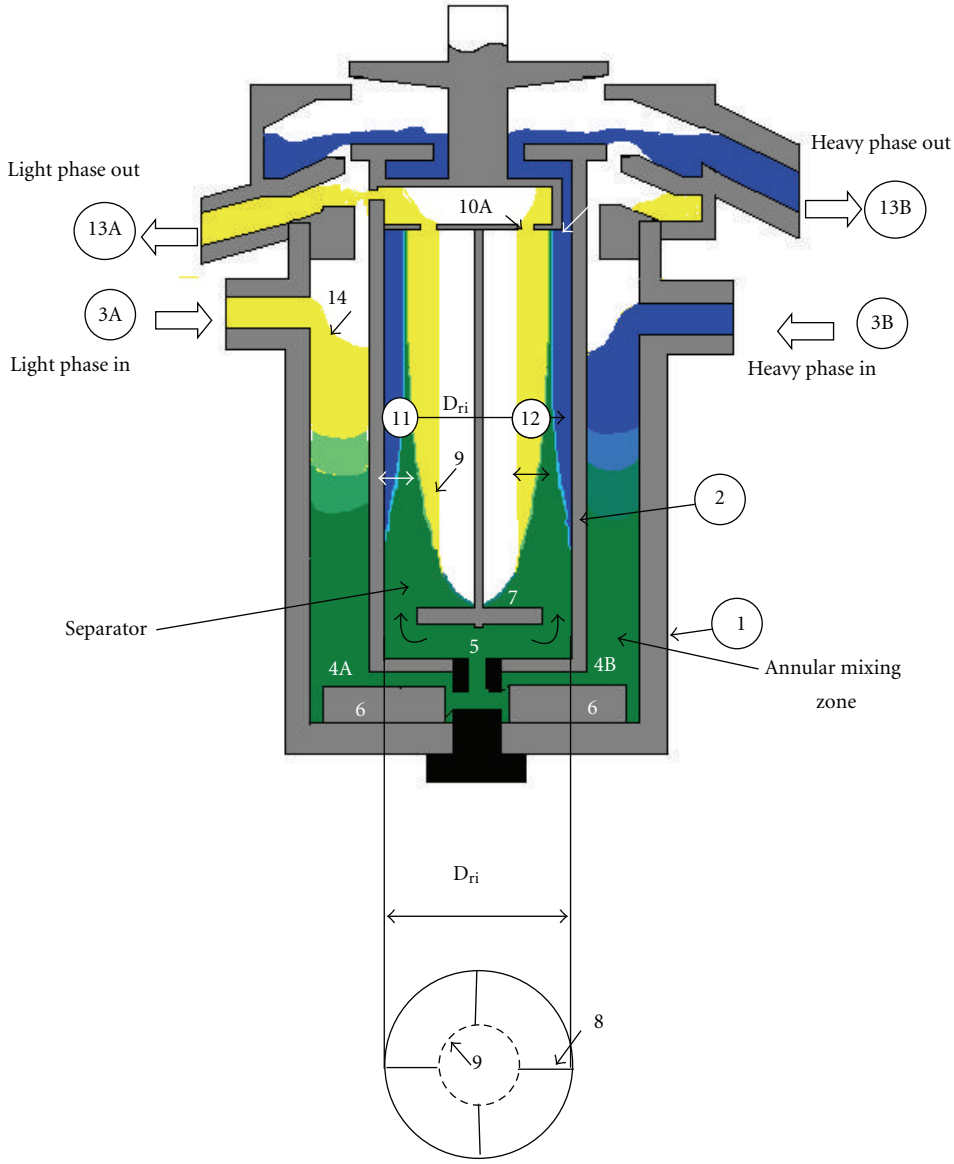

Figure 1: Schematic diagram of the annular centrifugal extractor (ACE) [6] (1) stationary cylinder, (2) rotating cylinder, (3A) light-phase inlet, (3B) heavy-phase inlet, (4A and B) Region below rotating cylinder, (5) central opening for rotating cylinder, (6) radial baffles on the stationary bottom plate, (7) deflecting baffle in the rotor, (8) vertical baffles in the rotor, (9) interface between air and light phase, (10A and B) overflow weirs for lighter and heavier phase, respectively, (11) clean width for heavy phase, (12) clean width for light phase, (13A and B) Outlets for light and heavy phases, respectively, (14) liquid level in the annulus.

20–600 kW/m^3) which results into a very fine dispersion of the two immiscible liquids. The dispersion flows downwards in the annular region (where the mass transfer occurs) and then flows radially inwards in the region below the rotating cylinder (points (4A) and (4B) in Figure 1) and finally enters the central opening (orifice) of the rotating cylinder (point 5). Baffles (6) are provided in the bottom region which are attached to the base of the outer cylinder (or in rare cases to the bottom of the rotating cylinder). The dispersion entering the central orifice gets deflected toward the wall by the horizontal deflecting baffle (7) provided close to the entrance. Above the level of (7) the rotor is provided with vertical baffles (8) so as to create several chambers ranging from 4 to 8. The rotating cylinder imparts to the liquid a practically rigid body rotation the inner surface of which has almost a vertical shape (9) because of high "g" (except a small parabolic portion at the bottom). The dispersion entering at the bottom gets separated as it moves upwards. The rate of separation depends upon the drop size distribution, their settling velocities under the centrifugal action ($r\Omega^2$), densities, viscosities, and coalescing behavior of the two phases. For complete separation (which is considered to be a flagship advantage of ACEs), adequate height needs to be provided for a given level of ($r\Omega^2$). After

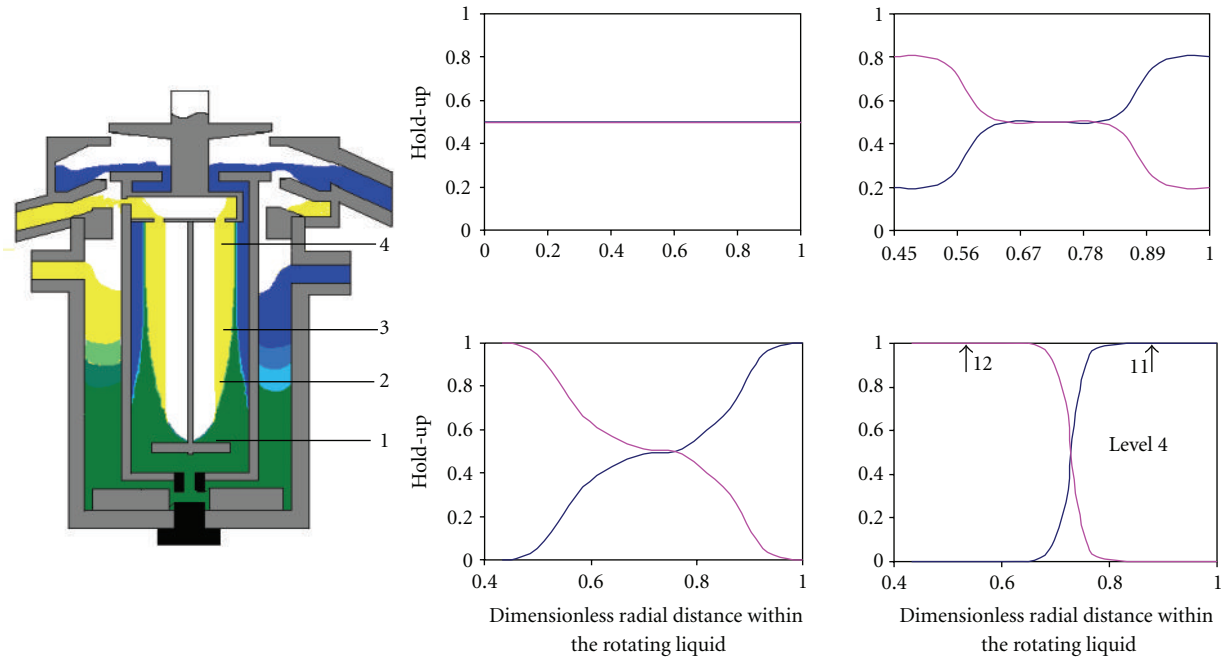

Figure 2: Variation of dispersion band in ACE [6].

complete separation, the overflow weirs [(10A) and (10B)] are provided in such a way that only very clean light and heavy phases pass over the respective weirs. The size and location of the weirs are provided in the hardware according to the relative flow rates of heavy and light phases and their corresponding clean widths (11) and (12). The flow of liquids from points (3A) and (3B) to (13A) and (13B) passes through the steps of extraction and separation.

Inside the rotor, the heavy and light phases are separated and the process of separation is schematically shown in Figure 2. It can be seen that, after the dispersion enters the rotor, the thickness of the dispersion band decreases as the dispersion flows upward. At point 4, complete separation can be seen to occur. The width of separation band at any location (say, point 3 in Figure 2) increases with an increase in flow rate and a decrease in interfacial tension. Further, the width decreases with an increase in the rotor speed and the density difference.

For a certain flow rate of aqueous phase, there is a maximum permissible flow rate of organic phase at which the dispersion band practically reaches the level of outflow weir (points 11 and 12 in Figure 1) and the carryover of mixed phase may occur in both or one of the outlet streams. This condition is known as flooding. The design of settler is based on the settling time of droplet of dispersed phase in the dispersion band. Hence, the characterization of dispersion band is very important in centrifugal extractors.

It is now known that the current practice of designing any process equipment (including annular centrifugal extractors) is closer to an art than the desired scientific procedures. Such a status is because of the complexity of fluid mechanics which includes three dimensional, turbulent, and multiphase nature of the flow in majority of process equipment. Therefore, since 1980, computational fluid dynamics (CFD) is increasingly being used for understanding the fluid mechanics in process equipment [3, 18, 31–57] and many others. Joshi and Ranade [58] have brought out the perspectives of CFD in terms of expectations, current status, and path forward. The following stepwise procedure has been recommended for rational and reliable design.

(1) Experimental measurements: flow visualization using particle image velocimetry (PIV), laser Doppler velocimetry (LDV), ultrasound Doppler velocimetry (UDV), tomography, phase Doppler particle analyzer (PDPA), and so forth.

(2) Computational fluid dynamics (CFDs) for the simulation of single phase or multiphase three-dimensional turbulent flow.

(3) Comparison between CFD predictions (step 1) and experimental measurements (step 2) for the validation of both the steps. The validation step is needed because the experimental technique as well as CFD have not reached stage of perfection.

(4) Development of relationship between the fluid mechanics and the design objectives such as mixing, axial dispersion, heat transfer, solid suspension, degeneration of proteins, and enzymes.

(5) Measurement of drop size distribution, effective interfacial area, mass and heat transfer coefficients, critical conditions for solid suspension, and so forth.

(6) Extensive comparison of steps 4 and 5 for the validation of these steps.

(7) Optimization: recommendations of design procedures and scaleup.

The above procedure has been used partially or fully by several investigators, for instance, for mixing [15, 19, 52, 53, 59–63], axial mixing [64–67], heat and mass transfer [68–73], gas induction [74–76], solid suspension [75, 77, 78], and enzyme deactivation [79].

In the present paper, we review the previous literature on CFD simulation of annular centrifugal extractors. In Section 2, qualitative description has been provided for the flow pattern in the annular and separator regions. Section 3 is concerned with the CFD formulation and the solution procedure. Further, the CFD simulation of single-phase flow in annular and separator regions has been described in Sections 4 and 6, respectively. The Sections 5 and 7 review the simulation of gas-liquid interface and two phase flow on the annular side whereas Section 8 is devoted for the simulation of multiphase flow on the separator side. An attempt has been made to bring out the current status of CFD simulations. Suggestions have been made for the future work in this area.

2. Hydrodynamic Characteristics

2.1. Centrifugal Instability and Taylor-Vortex Flow Regimes. At relatively low rotor speeds, the flow in the annular space is practically tangential because the viscous forces are dominant at low speeds. At high rotor speeds, when the centrifugal forces dominate the viscous forces, the flow patterns in the annular space results in an instability termed as the centrifugal instability, which leads to a wide and interesting scope of study into flow physics at micro-, meso- and macroscales. As the so-called Taylor-Couette flow attracts attention in the design and operation of efficient process equipment, nineteenth-century demonstrated ample studies that investigated the centrifugal instability occurring in these flows. Extensive reviews were presented by Koschmieder [80], Vedantam and Joshi [3]. A brief overview of the subject with some additional studies on this subject is presented here.

Couette [81] and Mallock [82] carried out drag experiments in concentric cylinder system and thus noted instability at certain rotational speeds. This was later explained by Rayleigh [83] for inviscid flows, wherein it was reported that flow is unstable only when the cylinders rotate in opposite directions. While, if they rotate in same directions, instability would result only when the angular momentum offered by the outer cylinder goes lower than the inner one. Taylor [84] theoretically analyzed the instability for viscous fluids, using linear theory of stability thus showing good agreement with experimental data. His analytical solution arrived at the definition of a dimension less number, which was later named after him as Taylor number (Ta). This number refers to the ratio of centrifugal forces to viscous forces and was expressed mathematically as

$$\mathrm{Ta} = \frac{4\Omega_i^2 d^4 (\vartheta - \eta^2)}{\nu^2 (\eta^2 - 1)}, \qquad \mathrm{Re} = \frac{R_i \Omega_i^2 d}{\nu^2}. \tag{1}$$

Various criteria for the onset of instability were arrived at and presented in the literature. A detailed discussion of all these criteria has been given by Vedantam and Joshi [3]. Jeffreys [85] used the linear theory of stability to study the analogy between Taylor-Couette flow and Rayleigh-Benard convection. These studies were limited to the narrow annular gaps. Then, wider gaps and a range of annular gaps were studied by many others [86–88]. Chandrasekhar [87] incorporated an axial flow in the linear theory of stability and thus found the transition from Couette flow (CF) to Taylor vortex flow (TVF) occurring at a number which was called as critical Taylor number ($\mathrm{Ta_{Cr}}$). He showed that the introduction of axial flow delays the occurrence of instability as

$$\mathrm{Ta_{Cr}} = 1708 + 27.15\mathrm{Re}_z^2. \tag{2}$$

The case of wide gaps was also addressed by Roberts [89], and the $\mathrm{Ta_{Cr}}$ was found to vary with the radius ratio as

$$\mathrm{Ta_{Cr}} = 1589.2\eta^{-1.0964}. \tag{3}$$

Stuart [90] used the nonlinear theory of instability for the first time to understand the variations in the formation of vortex patterns. This study was further followed by Davey [88], Coles [91], DiPrima and Eagles [92]. As the Ta increases beyond the $\mathrm{Ta_{Cr}}$, the flow structure changes from Taylor vortex flow to a wavy vortex flow (WVF). Upon further increase of Ta, this leads to a chaotic vortex flow (CVF), followed by fully turbulent Taylor vortex flow (TTVF). These various vortex patterns presented previously by Deshmukh et al. [26] are reproduced here in Figure 3, for ready reference of the reader.

The wavy nature of the WVF was found to be dependent upon the way in which the inner cylinder rotation was varied. Similarly, number of vortices also depended upon the startup conditions of experimentation [91]. Burkhalter and Koschmeider [93] carried out experiments to study the end effects on the vortex pattern. They found that the size of the end vortices increases with an increase in Ta, and the number of vortices decreases with an increase in the annular gap. In the classic work of Andereck et al. [94], flow maps were shown to depict the various flow regimes. They carried out flow visualization experiments using laser light-scattering technique. However, did not consider the continuous operation and hence there was an absence of the net axial flow. Lueptow et al. [95] brought out a flow map in the Ta-Re_z plane incorporating the axial flow. Koschmieder [80] carried out the flow visualization experiments to measure the wavelength of vortices formed by TTVF, upto a Ta of 40000 $\mathrm{Ta_{Cr}}$. It was also reported in his study that the vortex wavelength very much depended upon the experimental startup conditions.

Braun et al. [96] presented experimental and numerical results exploring various flow formations finally resulting into fully developed Taylor instability (500–1800 rpm). The experimental investigation uses the Full Flow Field Tracking (FFFT) method, to visualize the flow in longitudinal cross sections and at the same time correlate flow pattern observations to torque measurements. There experimental

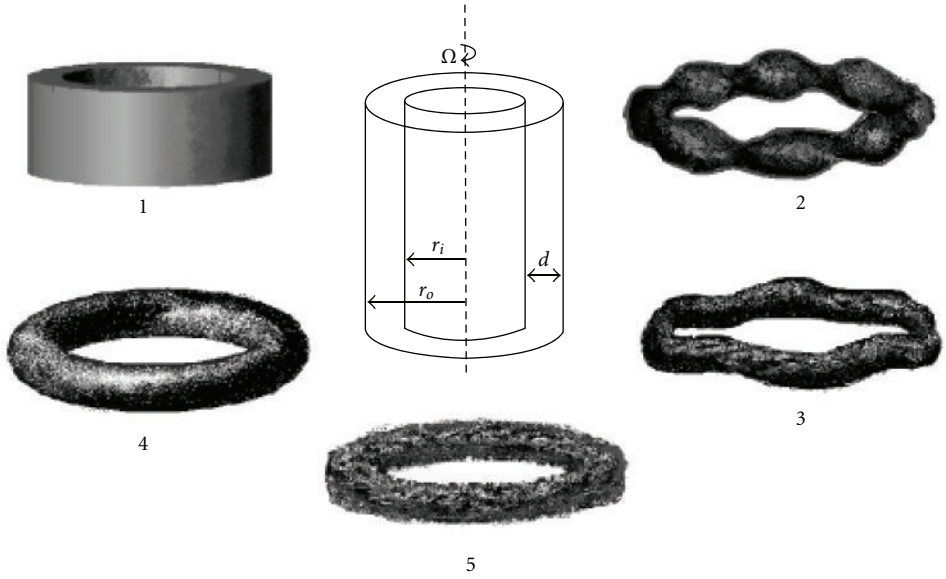

Figure 3: System of concentric cylinders and various vortex patterns in the absence of axial flow: (1) couette flow, (2) wavy vortex flow, (3) chaotic vortex flow, (4) Taylor vortex flow and, (5) turbulent Taylor vortex flow.

results indicated that incipient flow instabilities appear at lower speeds than the ones predicted by the Ta_{Cr}, and include formation of incipient Taylor cells that occupy only a part of the gap. The cells are separated by axially flowing narrow rope-like flowing streams that twist in a cork-screw fashion around the circumference, while separating the incipient cells. As the rotational velocities increase the Taylor cells keep growing until they occupy the entire gap. They also performed 3D CFD studies for the matching set of conditions and for the higher rotational velocities (1500–1800 rpm), where experimental studies were not possible. The torque computed by the numerical model was compared with the experimentally obtained torque and the two results were found to agree very favourably. Numerical simulation studies allowed an in-depth understanding of the flow mechanisms and trajectories inside the fully formed vortical Taylor instabilities (CFD simulations were performed using CFD-ACE+ commercial software).

Table 1 shows the geometrical details used for the CFD simulations in the past. Deshmukh et al. [26], in their paper on computational flow modeling and flow visualization in an annular centrifugal extractor, performed CFD simulations, and validated the modelled onset of centrifugal instability with the data of Rayleigh [83], Taylor [84], and Chandrasekhar [87]. They found that, as the rotation of outer cylinder increases, viscous forces become less important, as compared to the centrifugal forces and the Rayleigh criterion is arrived at, as an asymptote. In order to understand the effect of viscosity over a range of rotational speeds, they performed simulations over a wide viscosity range, thus capturing the gradual shift in stability curve from Taylor fluid towards the Rayleigh line.

Desevaux [97] studied the development of Taylor cells from Couette flow with a sudden start of the rotor, using a transient 3D CFD model. He thus proved the utility of CFD modeling to understand the propagation of Taylor cells. He used the data of Varechon et al. [98], for validation. The data used was from the laser tomography. The results were proven in line with the established data that vortex formation occurred after a Ta of 1700.

Saqr et al. [99] carried out five numerical experiments at different angular velocities to study the non-isothermal Taylor-Couette flow. They reported an uncharacteristic discontinuity locus numerically observed in the 2D nonisothermal Taylor-Couette flow at Re = 85 to 622. The Navier-stokes equations were solved in the discretised X-Y space using a finite volume, pressure-based approach for the unsteady flow between two concentric cylinders. The inner cylinder was subjected to constant heat flux and constant angular velocity, while the outer cylinder was fixed and maintained at constant temperature. The ratio between the outer and inner cylinder diameters was restricted to the ratio of sum of the cylinder diameters to the outer cylinder diameter (Golden Ratio).

Considering the studies reported on both experimental as well as numerical investigations, it is clear that CFD modeling could be used to understand the flow transition of Taylor instability. One extension of these studies would be to the modeling and simulation of secondary instabilities such as formation of azimuthal waves.

2.2. Separation Characteristics. The process of separation of the heavy and light phases inside the rotor is conceptually shown in Figure 2. It can be seen that, after the dispersion enters the rotor, the thickness of the dispersion band decreases as the dispersion flows upward. At point 4, complete separation can be seen to occur. The width of separation band at any location (say, point 3 in Figure 2) increases with an increase in flow rate and a decrease in

Table 1: Summary of geometric parameters used in the previous work.

Serial number	Authors	ACE dimensions				Simulation of		Number of Phases		Range of speed, r/s
		D_i (mm)	D_o (mm)	H (mm)	d (mm)	Annular region	Separator region	One	Two	
1	Zhu and Vigil, [153]	22.2	25.4	235		✓			LL	5–50
2	Wang et al., [170]	69.8	95.2	432		✓		✓		0.1–0.3
3	Vedantam et al., [5]	84	102	18	9	✓		✓		5–25
4	Wardle et al., [133]	50.8	63.4	37.76	6.3	✓		✓		50
5	Vedantam et al., [4]			16–225	1.5–15	✓		✓		0–15
6	Padial-Collins et al., [166]			150			✓		LL	16.67–50
7	Deshmukh et al., [26]	39		10–1000	2–15	✓		✓		0–20
8	Deshmukh et al., [132]	39	52	72		✓		✓		0–20
9	Wardle et al., [141]	50.8	63.4	81.3	6.3	✓			GL	60
10	Deshmukh et al., [119]		52	72		✓		✓		0–20
11	Wardle et al., [27]	50.8	63.4	81.3	6.3	✓			GL	60
12	Wardle et al., [143]	47.4		106			✓		GL	60
13	Sathe et al., [28]	39	49	57	5	✓			LL	2–26
14	Deng et al., [123]	36.8	60	60	11.6	✓		✓		3.35
15	Wardle, [145]	50.8	63.4	81.3 (Annulus) 106 (Separator)	6.3	✓			GLL (Annulus) GLL (Separator)	60
16	Gandhir and Wardle, [165]	47.4		106			✓		GL	60

*The orifice diameter d_o has not been included in the table as most the authors above have simulated the annular and separator regions separately and hence not in specified the orifice diameter d_o.

interfacial tension. Further, the width decreases with an increase in the rotor speed and the density difference.

For a certain flow rate of aqueous phase, there is a maximum permissible flow rate of organic phase at which the dispersion band practically reaches the level of outflow weir (points 11 and 12 in Figure 1) and the carryover of mixed phase may occur in both or one of the outlet streams. This condition is known as flooding. The design of settler is based on the settling time of droplet of dispersed phase in the dispersion band. Hence, the characterization of dispersion band is very important in the study of liquid-liquid extraction equipment such as mixer settlers, centrifugal extractors, among others.

Several investigations have been carried out to study the separation mechanism of liquid-liquid dispersion in a gravity settler [100–103]. The structure of dispersion band and the drop concentration at various levels in the dispersion band in the settler was studied experimentally for a wide range of parameters. The characteristics of dispersion band in a continuous settler are a function of dispersion band thickness and dispersion throughput. The thickness shows the variation of volume fraction of dispersed phase against the vertical distance from the coalescence front for various throughputs. Obviously, the dispersion band thickness increases with an increase in the throughput. The experimental evidences published are limited to the type of settler and no unified correlation exists to design the liquid-liquid settler for both batch and continuous types. Some of the researchers [1] estimated the settling time to characterize the interfacial area of liquid-liquid dispersion. However, this settling time did not fit into any of the existing dimensionless groups used in the interfacial area correlation to evaluate the separation capacity. Hence, there has been a need of a correlation for the design and scaleup of settling zone which is required to coalesce the liquid-liquid dispersions. This subject will be discussed in the following sections.

For correlating the separation data, Leonard [104] identified to characteristic time scales: (a) residence time of dispersion in separating zone of flow system (Q/V) or time for dispersion to break in batch systems (t_B); (b) time for a droplet to travel the thickness of the separating zone (settling time, T_S). If ΔZ is the thickness of dispersion band and V_S is the average hindered settling velocity of drops, the separation time is given by the following equation:

$$T_S = \frac{\Delta Z}{V_S}. \tag{4}$$

The value of V_S is proportional to g under creeping flow and $\sqrt{g}$ under turbulent conditions. Barnea and Mizrahi [100–102] have reported that the settling time is proportional to square root of acceleration (either gravity or centrifugal):

$$T_S \propto \sqrt{\frac{\Delta Z}{a}}. \tag{5}$$

Using (5), Leonard [103] defined the dispersion number as follows:

$$N_D = \frac{1}{T_S}\sqrt{\frac{\Delta Z}{a}}, \tag{6}$$

where N_D was denoted as dispersion number by Leonard [103]. For a flow system, the definition of N_D takes the following form:

$$N_D = \frac{Q}{V}\sqrt{\frac{\Delta Z}{a}}. \tag{7}$$

By introducing the concept of residence time t_R, the dispersion number can be expressed in the more general form:

$$N_D = \frac{1}{t_R}\sqrt{\frac{\Delta Z}{a}}. \tag{8}$$

In a gravity settler, acceleration is simply the acceleration due to gravity, g, and in a centrifugal settler, acceleration is given by

$$a = r\omega^2. \tag{9}$$

Acceleration varies within the centrifugal settler. Hence, the volume average acceleration is given by

$$a = \overline{r}\omega^2, \tag{10}$$

where

$$\overline{r} = \frac{\int_{ro}^{ru} 2\pi r^2 dr}{\int_{ro}^{ru} 2\pi r dr} = \frac{2}{3}\left(\frac{r_u^3 - r_o^3}{r_u^2 - r_o^2}\right). \tag{11}$$

From (7), it can be seen that the dispersion number is proportional to throughput for a given equipment size and a given acceleration field. It includes both the dispersion band thickness and time required for dispersion to settle. It also reflects the fineness of the drop size depending upon the time taken for the droplet to settle. The size of droplet varies with the speed of agitation or mixing. Hence, the dispersion number is a measure of efficiency of separation in liquid-liquid extraction equipment. It has been shown to be practically constant for wide range liquid-liquid systems [103]. It includes time for emulsion to break in such a way that both batch and flow systems give the same value of dispersion number for a particular liquid-liquid system.

Recently, Tamhane et al. [105] have performed separation experiments under gravity and centrifugal conditions over a wide range of parameters ($120 < \Delta\rho < 600\,\text{kg/m}^3$, $3 < \sigma < 58.3\,\text{mN/m}$, $1 < \mu_C < 12.2\,\text{mPa.s}$, $0.6 < \mu_D < 12.2\,\text{mPa.s}$, $0.05 < D_i < 0.25\,\text{m}$, $0.005 < (D_o - D_i) < 0.025\,\text{m}$, $10 < N < 40\,\text{r/s}$). They have proposed the following correlations for the dispersion number:

Gravity settling

$$N_D = 0.0562\left(\frac{\sigma^3\Delta\rho}{\mu_C^4 g}\right)^{0.059}\left(\frac{C}{D}\right)^{-0.111} \times \left(\frac{\Delta\rho}{\rho_C}\right)^{0.101}\left(\frac{\mu_C}{\mu_D}\right)^{-0.211}; \tag{12}$$

Annular centrifugal extractor

$$N_D = 0.1\left(\frac{\sigma^3\Delta\rho}{\mu_C^4 g}\right)^{0.036}\left(\frac{C}{D}\right)^{0.019}\left(\frac{\Delta\rho}{\rho_C}\right)^{0.174} \times \left(\frac{\mu_C}{\mu_D}\right)^{0.074}\left(\frac{a}{g}\right)^{-0.086}\left(\frac{Q}{ND_i^3}\right)^{0.95}. \tag{13}$$

As an example of the use of dispersion number in design of ACE, let us fix the total throughput to $6.5\,\text{m}^3/\text{h}$. The rotor speed is kept to a typical value of 30 r/s. From (7), we can see that N_D depends on the variables Q, V, ΔZ, and a. V is in turn a function of the rotor height H. As a general thumb of rule, $H \sim 2.5R_i$, where R_i is the rotor radius. Now, $V = \pi R_i^2 H$. Thus, $V = 2.5\pi R_i^3$. Also, $a = \omega^2 R_i$. Hence, at 30 r/s, $a = 35495R_i$. Further, while designing the dispersion band thickness at maximum throughput, the fluid is thought to occupy the entire rotor. Hence, ΔZ in this case is equal to R_i. Thus, (7) reduces to the form:

$$N_D = \frac{9.54 \times 10^{-6}}{R_i^3}. \tag{14}$$

Taking a value of N_D to be 0.00075, we get the value of R_i equal to 0.119 m. Thus, D_i is equal to 0.238 m. The tested capacity of a 250 mm rotor ACE is indeed $6.5\,\text{m}^3/\text{h}$, which is consistent with the aforesaid procedure.

3. CFD Formulation and Solution Procedure

Performance of annular centrifugal extractors (ACEs) crucially depends on underlying fluid dynamics and mixing. Even single-phase flow through such ACEs exhibits rich physics and multitudes of flow regimes. Presence of multiple phases leads to even complex flow structures. The physical construction and operation of ACEs are discussed in previous two sections. On the face of it, the underlying complexities appear almost intractable and the task of computational modeling of ACEs looks truly daunting. Despite the apparent intractability, computational modeling has, however, potential to offer better insight and useful information for evolving design guidelines. Various investigators have attempted to develop computational fluid dynamics based models for carrying out simulations of flow in ACEs. The work done so far is critically reviewed in Sections 4 to 7. In this section, general approach and framework for examining such CFD models and simulations is discussed.

Some of the key aspects discussed in the Sections 1 and 2 are reexamined here in light of formulating appropriate modeling framework. Please note that typical power dissipation per unit mass in ACEs is significantly higher (in the range of 20–600 kW/m^3) than classical stirred tanks. The typical tip speed of inner rotating cylinder is in the range of 1 to 25 m/s. This results into a very fine dispersion of the two immiscible liquids. Flow in the annular space is turbulent and typical Kolmogorov length scales are in the range of 10^{-6} to 10^{-5} m. The ratio of Kolmogorov length scales to annular gap is, therefore, in the range of 10^{-5} to 10^{-3} m. The flow within the annular space becomes unstable and exhibits

many diverse flow regimes. There may be a free surface in the annular space depending upon the flow rates, dispersion process, and specific construction of ACE. The presence of free surface makes the problem even more complex. For estimating the extraction, it is important to capture size of the dispersed phase particle, location of free surface and axial mixing within the annular space.

The dispersion enters the inner rotating cylinder from the bottom orifice. Baffles which guide the dispersion towards inner cylinder via orifice are one of the key design components. Computational flow models can provide useful insight on this. In this region, the flow is characterized as turbulent-dispersed multiphase flows. Usually there are baffles (horizontal as well as vertical) in the inner rotating cylinder. The rotation of inner cylinder creates strong body force and cause phase separation. The rate and extent of phase separation depends upon the drop size distribution, difference in densities and viscosities of two immiscible phases and coalescing behaviour. Appropriate sizing of inner cylinder and outflow weirs is critical for adequate separation of phases. Typically centrifugal acceleration experienced by dispersed phase particles in the inner rotating cylinder is in the range of 1000 to 5000 m/s^2. This acceleration causes coalescence and separation leading to stratified flow regime in inner rotating cylinder. Flooding may occur if the phase separation does not occur adequately and may lead to the carryover of mixed phase in both or one of the outlet streams. It is important to gain better understanding of regime transition and phase separation for obtaining a handle on separation efficiency of ACEs.

Considering the large number of design variables available for tuning the performance of ACEs, it is useful to develop computational models to simulate fluid dynamics of ACEs and use the simulated flow fields for drawing useful design guidelines. Most of the early modeling efforts were primarily focused on descriptive correlations of experimental data. The dimensionless dispersion number described above was developed in order to predict the maximum throughput of a contactor for a given set of immiscible fluids and a fixed rotor speed. Significant effort was also put forth in the development of a computational model which could aid in the design of contactor weirs by calculating the necessary weir sizes given the properties of the two phases. A descriptive model for the height of the liquid in the annulus as a function of rotor speed was also developed. In recent years, significant efforts have been carried out to exploit recent advances in computational fluid dynamics (CFD) to gain better understanding of ACEs. CFD based models and simulations have in principle potential to provide qualitative as well as quantitative analyses of the flow within ACEs. Such analysis may enable greater understanding of and confidence in scaled-up designs which would be used in pilot and full-scale operational facilities. However, the potential benefits strongly depend on how well the key aspects briefly reviewed here are represented while formulating CFD models. Prevailing approaches for CFD modeling are briefly reviewed here along with an outline of the challenges to modeling these flows. The obtained results and observations from various studies are critically reviewed and discussed in Sections 4 to 7. It will be useful to examine key design issues of ACEs and discuss possible CFD approaches to address those issues. It will be useful to begin the discussion from the inlets.

Two immiscible feed liquids enter ACE via two separate inlets connected to the annular region between the two cylinders (see Figure 4(a)).

The spinning of the rotor creates a dispersion of the two immiscible liquids. The dispersion flows downwards in the annular region (where the mass transfer occurs) and then eventually enters the inner rotating cylinder via bottom opening (point 5 in Figure 4(b)). The liquid height in the annular region is one of the critical design parameters. For a specific configuration, this liquid height in the annular region determines the throughput of the mixing zone. While the throughput of a given contactor is typically limited by the capacity for complete separation of the two phases within the rotor such that there is minimal other-phase contamination in the respective outlets, another limiting case is if the dispersion in the annulus fills the mixing zone and overflows into the organic collector ring. Even if the liquid height under nominal conditions is acceptable, flow transients and changes in liquid height due to phase inversion make the annular liquid height an important factor during operation.

Another important and relevant issue in the annular region is possible entrapment of air in the liquid-liquid dispersion. Since the region being open to air, air bubbles may get entrained and entrapped in the annular region. This will lead to reduction in drag, and thus a reduction in energy dissipation. Such entrapped bubbles have been observed in the flow visualization experiments. The liquid height as well as entrapped bubbles also influence flow characteristics in the annular region including axial mixing as well as mass transfer characteristics. It is, therefore, important to review CFD approaches needed to estimate these key desired characteristics in the annular region.

It can be seen that the fluid dynamics of annular region is very complex involving creation of dispersion in presence of multiple free surfaces (liquid-liquid and gas-liquid) and intense turbulence in a geometrically complex shape with moving boundaries. It is almost impossible to make "a priori" predictions of such a complex flow. However, judicious use of CFD models can provide very useful insights and guidelines for design purposes. The overall flow structures and axial mixing can be reasonably estimated by making a pseudohomogenous assumption to represent liquid-liquid dispersion. The first cut solution may be obtained by even ignoring the free surface and simply using single-phase flow simulations. These single-phase simulations will provide useful estimates of energy dissipation rates as well as axial mixing in the annular region. The estimates of energy dissipation rates may be then used to estimate representative droplet diameter to estimate mass transfer coefficients. The Eulerian-Eulerian (EE) approach can then be used to understand possible influence of slip between two liquid phases. Please note that more often than not effective drag in liquid-liquid dispersions will be a strong function of Kolmogorov length scale (energy dissipation rate). Appropriate correlations of effective drag coefficients

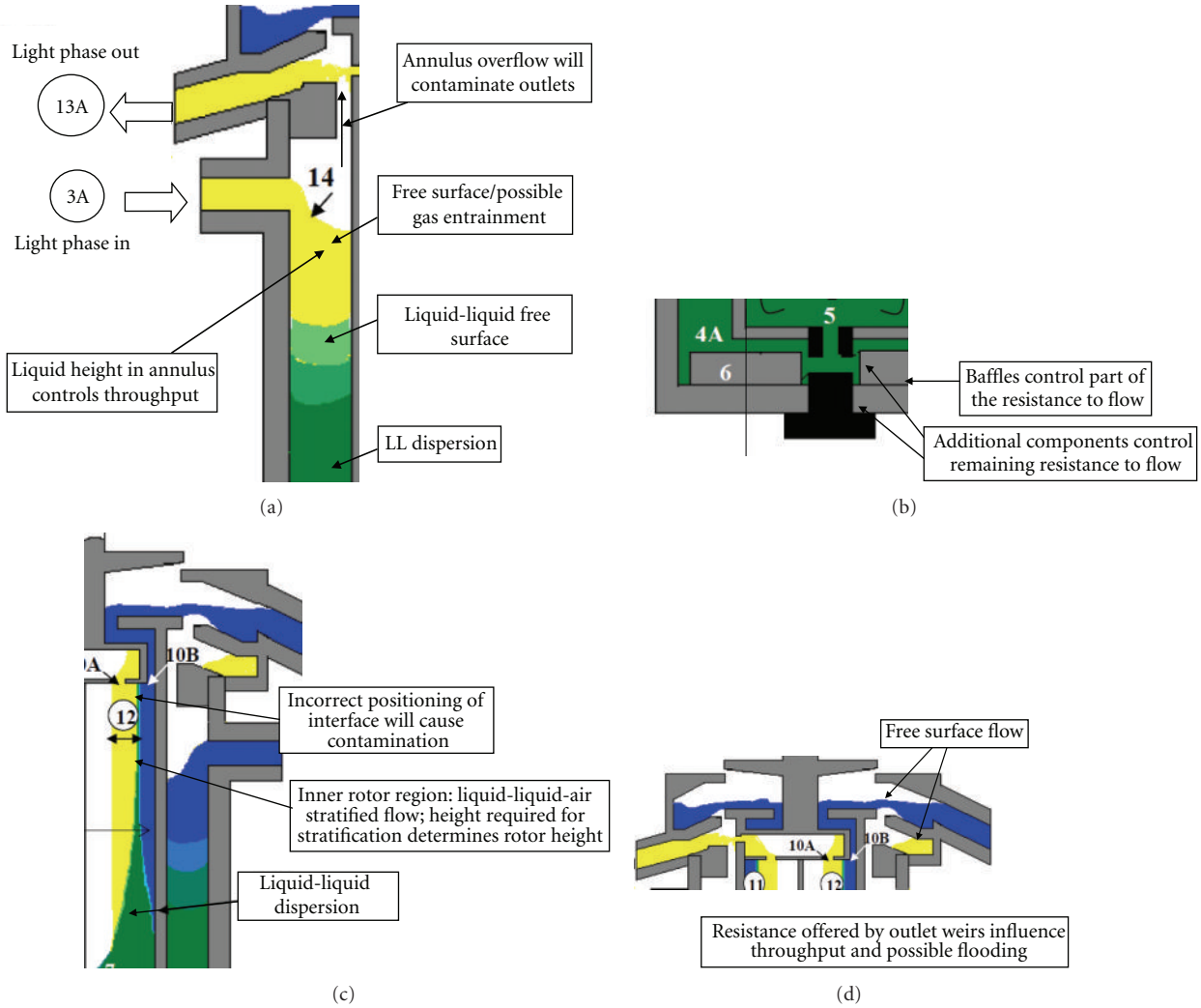

Figure 4: (a) Schematic representation of the inlet and outlet sections of ACE, (b) schematic representation of the bottom vanes and resistance, (c) dispersion band and sections tapping light and heavy phases in the separator region, (d) Heavy-phase weir and free surface flow at the top at the point of collection.

should, therefore, be used while developing EE based CFD models for ACE. These models can then be combined with volume of fluid (VOF) approach to capture free surface as well as possible entrainment of gas phase. This last approach invariably required 3D simulations and, therefore, is very compute intensive. The approach can, however, provide useful information on possibility of overflow of annular region (and contamination with the organic phase outlet) as well as entrapment of gas bubbles. More information about the EE and VOF approaches may be found in Ranade [106]. More information on hybrid approach (EE with VOF) may be obtained from the work of Kuipers and coworkers [37–41].

The flow in the bottom region of ACE is essentially controlled by the geometrical configuration of the bottom region (see Figure 4(b)).

The key design aspect of the bottom region is to provide appropriate resistance to flow from annular region to inner rotating cylinder. This is realized by providing baffles (fixed in number, shape, size, and location for a given configuration of ACE) as well as additional moving components to realize ability to manipulate resistance during the ACE operation (position of these can be modified to realize better operating conditions in ACE). Since the key design issue is to estimate flow resistance or pressure drop offered by the bottom region, single-phase CFD simulations using the pseudohomogenous fluid (representing liquid-liquid dispersion) are adequate. The choice of turbulence models (since the geometry is quite complex) and use of adequate number of computational cells are crucial to obtain accurate estimated of flow resistance and key features of flow in the bottom region of ACE. Such CFD models can be used to evolve appropriate guidelines for manipulating flow characteristics of ACE by influencing flow in the bottom region of ACE.

The flow in the inner rotor region is again quite complex involving significant changes in the flow characteristics.

The liquid-liquid dispersion enters the rotor and eventually transitions to stratified flow regime because of the strong centrifugal action.

In liquid-liquid stratification studies, the two-phase flow is another variation of a single-phase flow that explores the effect of interface on the vortex flow. A significant challenge with free-surface modeling techniques is that they are inherently mesh dependent; only interfacial features that can be resolved on the mesh can be captured. As a further limitation, such methods are time dependent by nature and are limited by the Courant flow number, in turn showing the dependency of time step on mesh spacing. The regime transition is inherently a complex problem. The existing VOF based approach may, however, be used to obtain broad estimates of height required for realizing stratified layers. A combination of EE and VOF will be useful to simulate the flow in the inner rotor region of ACE.

Closely linked with the flow characteristics of the inner rotor, the flow in the outlets and associated weirs is equally crucial to understand for realizing stable operation of ACE. The key features of flow in the outlet region are as follows.

The pressure drop across outlet weirs influences number of design parameters of ACE. CFD-based studies help in understanding the flow in the weir region and, therefore, several other key design parameters of ACE. Until recently, CFD modeling techniques had not been applied to the rotor design in ACE. However, a useful analytical approach was demonstrated for determining the proper dimensions of the weirs based primarily on experimental correlations and hydrostatic balance arguments [107]. While this method has been generally quite successful for rotor sizing of contactors with an open upper weir (and the obsolete air-controlled upper weir), some experiments with "closed" upper weir systems have produced behavior which cannot fully be explained by the existing theoretical models. One such unexplained behavior is the elevated throughput that has been observed for large upper weir sizes in these units. This same behavior has also been observed in larger units of this design. VOF approach or even a single-phase approach may be used to estimate pressure drop across outlet weirs of ACE. CFD modeling can provide useful insights in resolving such issues.

Better understanding of the flow within the rotor and specifically the flow over the weirs requires full simulation of the complex rotor and weir geometries and analysis of the liquid free surface flow. Further, such hydraulic simulations can calculate important flow quantities which characterize the rotor and weirs such as the zero-point flow rate. Zero-point flow rate refers to the point wherein, due to excess flow rate coming into the rotor, the liquid volume maintained in the rotor increases so much that the liquid starts to come out of exit ports without getting separated. These kinds of studies are barely reported in a couple of papers until date. In practice, the zero-point flow rate is used to verify fabrication consistency of a set of rotors with the same specifications, such as might be used in a multistage bank of contactors.

This brief review of CFD approaches relevant to different aspects of ACE design and operation indicates the usefulness of computational flow models. Some of the applications of these are discussed in the subsequent sections. The governing equations for single phase flows, the Eulerian-Eulerian approach and volume of fluid approach may be found in many text books (for example, Ranade [106], Ranade and coworkers [18, 19, 54, 108–110], and manuals of commercial CFD vendors). These are, therefore, not repeated and discussed here. Appropriate boundary conditions need to be formulated for connecting the generic CFD model to the specific configuration under consideration. It is often essential to make judicious use of constant pressure, velocity inlet and outlet boundary conditions to effectively represent various sections of ACE. The boundary conditions used by different investigators are reviewed in the subsequent sections while discussing the results available in the published literature.

The quality of simulated results using CFD models of course also crucially depends on numerical implementation of selected model equations. Table 2 gives a summary of key numerical parameters (like the number of grids used, method of discretization and the solution procedure) used by various investigators. It is essential that adequately fine mesh (compared to relevant space scales of the considered ACE) is used along with the higher order discretization schemes. The published CFD results are reviewed in the following sections in light of this brief review on formulation and solution of CFD models.

4. CFD Simulation of Single Phase Flow on the Annular Side

4.1. Velocity Profiles in Presences/Absence of Axial Flow. The earliest studies on velocity profiles date back to that of Taylor [84], who plotted radial velocity distribution against the onset of centrifugal instability and also determined the vortex spacing from both analytical and experimental studies. Most of the studies reported till date have presented results on flow field determination and flow regime classification. While the mixing zone in the annulus extends along the entire length of the annulus, initial studies focused on neglecting the end regions of the annulus, thus reporting the flow field for larger aspect rations. The information typically obtained was the flow regimes and the vortex patterns. Later, with advances in methodology, end effects were also considered.

For highly turbulent regimes, Parker and Merati [111] used Laser Doppler Anemometry (LDA) to measure three components of mean velocity and turbulent intensity at various circumferential planes. They studied the end effects on vortices for aspect ratios of 4 and 20. Baier [112] carried out CFD modeling to determine vortex velocities for various operating conditions. Haut et al. [113], also carried out CFD simulations, in the annular region in a horizontal corotating cylinder system. They used the k-ε turbulence model to incorporate turbulence effects in wavy vortex flow and turbulent Taylor vortex flow. Particle image velocimetry (PIV) was used to determine average and instantaneous velocities.

Table 2: Some details of CFD simulations in previous work.

Serial number	Authors	Number of grids	Method of discretization*, **			Multiphase model used
			Momentum	Pressure-velocity coupling	Pressure equation	
1	Zhu and Vigil, [153]	30 (radial) × 300 (Axial)				ASM (Fluent 5.0)
2	Wang et al., [170]					(Fluent 6.0)
3	Vedantam et al., [5]	3D 70000 Hexahedral	First order upwind	PISO	PRESTO	VOF (Fluent 6.1)
4	Wardle et al., [133]	3D 588484 Tetrahedral	First order upwind	SIMPLE	Standard	(Fluent 6.1)
5	Vedantam et al., [4]	2D 20000	First order upwind	SIMPLE	Pressure staggering option (PRESTO)	(Fluent 6.1.2)
6	Padial-Collins et al., [166]					(EE) (CartaBlanca)
7	Deshmukh et al., [26]	2D 20000	QUICK upwind	PISO	Pressure staggering option (PRESTO)	(Fluent 4.5, 6.0)
8	Deshmukh et al., [132]	3D 600000 Hexahedral	QUICK	PISO	PRESTO	(Fluent 6.2.16)
9	Wardle et al., [141]	3D 286000	First order upwind	PISO		VOF (Fluent 6.3)
10	Deshmukh et al., [119]	3D 600000 Hexahedral	QUICK	PISO	PRESTO	(Fluent 6.2.16)
11	Wardle et al., [27]	3D 800000 Tetrahedral				VOF (Fluent 6.3)
12	Wardle et al., [143]	311000 Tetrahedral (Annulus) 160000 Tetrahedral (Separator)				VOF (Fluent 6.3)
13	Sathe et al., [28]	3D 600000 Hexahedral	Second order upwind	SIMPLE	PRESTO	(EE) (Fluent 6.3)
14	Deng et al., [123]	3D 600000 Tetrahedral	First order upwind	SIMPLE	Standard	(Fluent 6.3.06)
15	Wardle, [145]	650000—2.5 M Polyhedral	First order upwind	PISO		VOF (Open FOAM-1.6)
16	Gandhir and Wardle, [165]	3D 586846 Polyhedral	First order upwind	PISO		VOF (Open FOAM-1.6)

*Most of the authors, *except from the group of Joshi and coworkers*, have only specified that fluent (specific version) has been used for the CFD simulations. They have *Not* mentioned the various model parameters used for the simulations.
**The underrelaxation factors have Not been specified by most of the authors.

Deshmukh et al. [26] carried out both 3D CFD and experimental measurements, and made an extensive comparison with the data from the literature. They have covered a wide range of annular gaps, rotation ratios, and net axial liquid velocities. Energy balance also was established for various operating conditions. In case of counter-rotating cylinders, an additional set of vortices was found along the length of the annulus beyond a certain Ta_{Cr}. For the case of the annular centrifugal extractor, they observed elongated vortices at both the ends of the annulus; however, they concluded that the vortex at the lower end shows more elongation. Further, the flow was found to be tangential in the region below the rotating cylinder. Sathe et al. [28], in their study of two-phase liquid-liquid flow, carried out CFD simulations for single phase and compared the data with the PIV measurements for a vertical configuration. They compared their simulation data with the vortex spacing and found the comparison to be inline with measured data.

4.2. Axial Mixing and Residence Time Distribution. Axial dispersion in Taylor-Couette flow has been investigated in the past and reported in the literature. Vedantam and Joshi [3] have summarized the axial dispersion studies in Taylor-Couette contactors for various flow regimes. In laminar flows, RTD experiments and the description of axial dispersion either by one parameter that includes dispersed plug flow model or tanks in series model has been used or a two parameter model has been used [114–116]. Normally, it has been shown in most studies that laminar Taylor vortex regime usually is depicted by well-defined vortices.

Kataoka et al. [114], for the first time provided a basis for treating each vortex as a well-mixed reactor. They performed two-point RTD measurements and concluded that there is no vortex intermixing. Thus, at a higher aspect ratio (implying that end effects could be neglected), the overall flow was expected to go close to plug flow behavior. Desmet et al. [117, 118] investigated mixing in laminar flows and concluded that under laminar flow conditions, intravortex transport is slow compared to intersvortex transport and indicated that a single vortex cannot be treated as a well-mixed reactor. However, as the Taylor-vortex flow reaches the flow regime of turbulent Taylor vortex flow, intravortex flow is prominent than the intervortex flow. Vedantam et al. [5] used

CFD for estimating the mixing time and RTD in a Taylor-Couette flow. They also obtained very good agreement with the experimental observation reported previously in the literature. However, their study was confined to a lower range of Ta, which is unlikely to be applied for highly turbulent regimes needed in the study of annular centrifugal extractors.

Deshmukh et al. [119] studied RTD for the annular region of the annular centrifugal extractor experimentally as well as computationally. They developed an experimental technique capable of picking quick response. The convective motion was shown to control the rate of mixing, and the role of turbulent diffusion was found to be small. They concluded that the RTD studies indicated the existence of a single-back-mixed stage, inspite of the presence of multiple vortices in the annulus. Further, the numbers of tanks in series were found to be dependent on the aspect ratio used in the geometry. Figure 5 shows the flow patterns and turbulent properties at 30 rev/s used by them, at the center of the annulus. Details of the reproduced figure are mentioned within the figure caption. Their work also indicated an attempt toward reducing the axial mixing by providing radial baffles, which practically leads to a plug flow kind of behavior.

4.3. Effect of Internals on the Flow Field. In general, baffles play a significant role in engineering devices. Baffles enhance mixing efficiency in a tank or a batch oscillatory column [120, 121] and they are used to increase permeate flux in membrane filtration [122]. Deng at al. [123] carried out characterization of Taylor vortex flow in a short column with a wide gap and concluded that the vortex flow was sensitive to boundary conditions. Several modified boundaries including end wall effects [124] were studied. Some studies included varying the radius of the inner cylinder [125] and also asymmetric boundary conditions [126]. All the above studies were seen to affect the vortex formation. However, there were very limited results which were presented in the above literature with regard to baffled devices in Taylor vortex flow or annular centrifugal extractor. The work in [127] introduced a baffle in the upper part of the rotating cylinder electrode cell. But this was done in order to avoid any bubble formation in the annular region noting that, up to a speed of 3000 rpm, no bubbles were formed. Some studies were reported on the rheology of slurries using a Debex viscometer [128]. They also attributed the formation of Taylor vortices to the existence of baffles. Clark [129] carried out experiments in electrochemical reactor for electrodeposition in an eco-cell. Taylor vortices were also observed as a cascade of cells separated by baffles.

Sczechowski et al. [130], showed that the introduction of horizontal baffles does not change the axisymmetric feature of the Taylor-Couette flow. Instead, they are shown to provide additional surfaces to confine the vortex flow. Horizontal baffles were found to affect the vortex size. In an infinitely long column, the diameter of an individual vortex was found to be approximately equal to the annular gap.

Loureiro et al. [131], carried out both numerical and experimental studies to understand the Taylor-Couette instabilities in flows involving Newtonian fluids as well as power-law fluids. The flow inside a horizontal annulus due to the inner cylinder rotation was studied. The bottom of the annular space was partially blocked by a plate parallel to the axis of rotation, thereby destroying the circumferential symmetry of the annular space geometry. This flow configuration was encountered in the drilling process of horizontal petroleum wells, where a bed of cuttings is deposited at the bottom part of the annulus. The velocity field for this flow was obtained both numerically and experimentally. In the numerical work, the equations which govern the three-dimensional, laminar flow of both Newtonian and power-law liquids were solved via a finite-volume technique. In the experimental research, the instantaneous and time-averaged flow fields over two-dimensional meridional sections of the annular space were measured employing the particle image velocimetry (PIV) technique, also both for Newtonian and power-law liquids. Their study was focused on the formation of secondary form of distorted Taylor vortices. Deshmukh et al. [132] examined flow patterns and axial back mixing in the presence of radial baffles in the annulus and concluded that the horizontal radial baffles can reduce the axial mixing in turbulent Taylor-Couette flow.

Deng et al. [123] presented a study on Taylor vortex flow in between a rotating inner cylinder and a stationary outer cylinder with vertical as well as horizontal baffles. They found that, upon the introduction of vertical baffles, the axisymmetric vortex nature is eliminated thus leading to a three dimensional flow pattern, including the recirculation flow in the radial-azimuthal plane and periodic variation of the vertical position of the vortices. The horizontal baffle was found to separate the original fluid column in compartments, and the length of the vortices inside was found to be a variable in a certain range to fit the compartment dimension. They found that the number, position, and width of the baffles do affect the vortex structure in the annulus. Figure 6 shows the Taylor vortices obtained in presence of horizontal baffles. With two horizontal baffles in the annulus, the flow pattern is largely affected by the baffle width and the distance between the two baffles. This study provided a better understanding of Taylor vortex flow in presence of internal baffles, which will be important for practical applications of Taylor vortex devices.

4.4. Challenges in Validation Data Generation for Flow Visualization. The flow in the ACE is generally turbulent, unsteady, and it most likely could consist of liquid-liquid-gas phases, thus increasing the complexity involved in the modeling as well as data generation. Under typical conditions, the flow in the mixing region opaque; thus, laser-based, optical techniques are limited to interrogation of the near-wall regions only. Optical access to the flow inside the rotor is also obviously restricted although transparent rotors have been fabricated.

Due to the challenges of quantitative measurement of flows in actual contactor configurations at typical operating conditions with multiple phases, the available experimental data in the literature tends to be for simplified geometries, single phase operation, and/or reduced rotor rotation rates. While this provides a means of more direct comparison with CFD simulations, if the test conditions are greatly varied

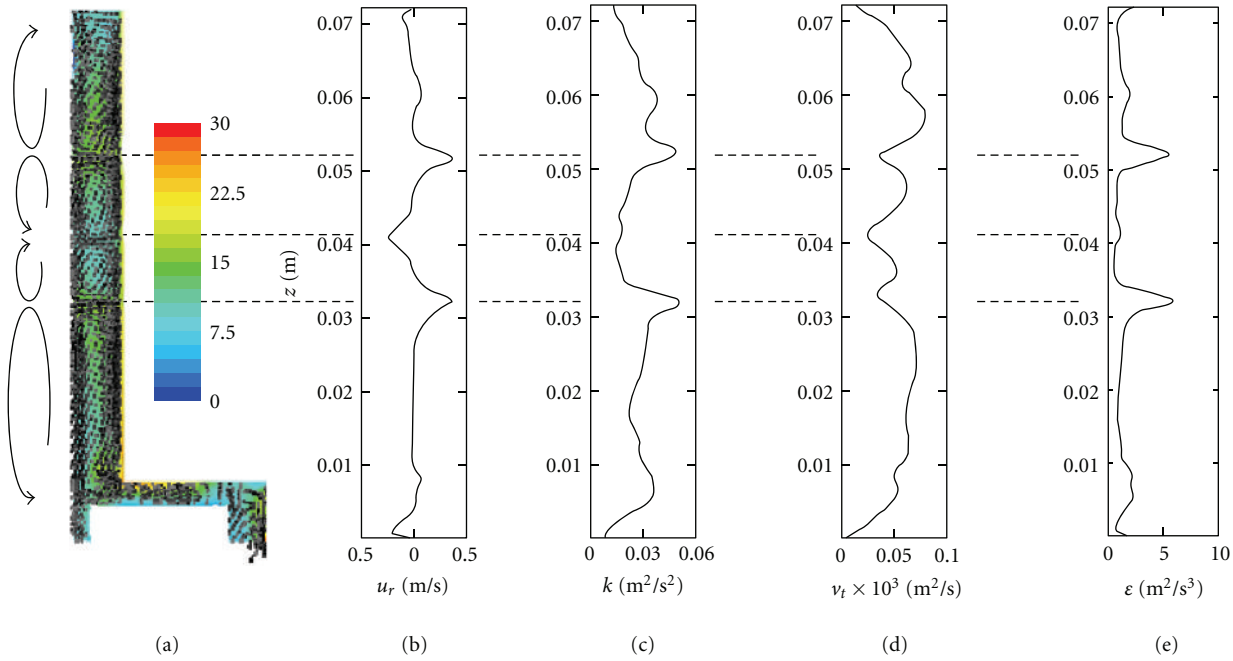

FIGURE 5: Flow patterns and turbulent properties at 30 r/s and total flow rate 4.16 mL/s at the center of annulus: (a) contours of turbulent intensities (%); (b) radial velocity profile; (c) turbulent kinetic energy profile; (d) turbulent viscosity profile; (e) turbulent kinetic energy dissipation profile [119].

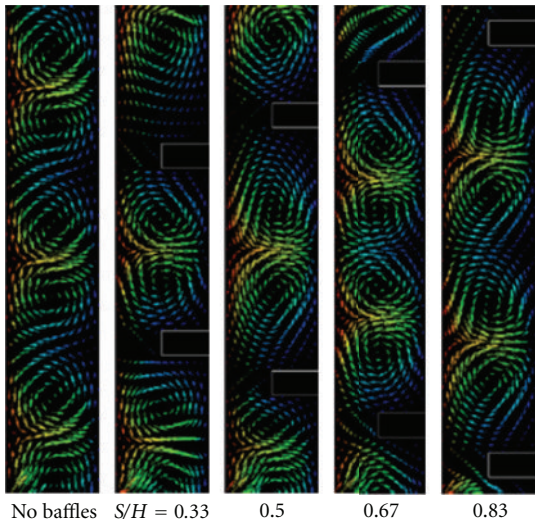

FIGURE 6: Flow patterns in presence of horizontal baffles in the annulus [123].

from realistic ones, there is the problem of extrapolating the "validation" of the simulation at reduced conditions to one at realistic conditions where the flow regime may be substantially different such that the models are no longer valid.

The issue of turbulence always requires attention. Though LES and full RSM modeling methods are available, RANS solution methods such as k-ε model are still widely used owing to their less computational expense. Further, it was shown in the literature that unsteady RANS solution methods capture both qualitatively and quantitatively complex flows which are not statistically stationary with much more accuracy, as compared to steady RANS solutions [133–135].

5. CFD Simulation of Gas-Liquid Interface on the Annular Side

While a simplified, single-phase approximation of the flow in the annular zone of a centrifugal contactor as described in the previous Sections (4.1 to 4.4) yields some useful insights and provides a reduced complexity condition for both simulation and experiments, it is, nevertheless, unable to capture important characteristics of the flow in the actual device as it is typically configured. In particular, the annular region of the centrifugal contactor is not liquid full due to the upper end being open to the collector ring region and outlet channels which are maintained at zero gauge pressure to ensure steady flow between stages. Thus, even for hydraulic operation with a single liquid phase, the flow from the inlets into the annular region can be by droplets or rivulets down the housing wall or rotor depending on operational conditions. Thus, free surface effects dominate the annular region flow and make it quite different from standard closed system Taylor-Couette flow. While annular centrifugal extractor designs do exist [136] in which the effect of the free surface and air drawdown into the annular region has been reduced, the majority of available designs are subject to an "open" annulus with free surface flow.

The effect of an upper free surface on Taylor-Couette flow between vertically oriented concentric cylinders has been primarily studied for low to moderate Reynolds numbers [137–139]. For example, Watanabe et al. [137] explored—both experimentally and computationally—rotation rates up to Re = 2000 where free surface instabilities are present but extremely mild compared to those found under typical conditions (Re > 50,000) in centrifugal contactors. The influence of the free surface was seen as a slight variation in the shape of the upper most Taylor-Couette cell which was also found to be slightly larger than lower ones. As seen also in Deshmukh et al. [132], the number of cells was also found to be dependent on the startup procedure with a sudden start tending to result in a larger number of Taylor cells than a linear ramping of the rotation rate to the final state. Mahamdia et al. [138] experimentally explored the effect of a free surface on TC flow at low rotation rates and identified secondary instabilities near the free surface.

Due to the added complexity of the free surface at high rotation rates, experimental studies of flows in such conditions are few. Mujica and Lathrop [140] have experimentally observed the instabilities of turbulent free-surface flow in an annular device for high Reynolds numbers (Re $\sim 10^6$) and have observed large-scale "gravity-wave" oscillations in liquid height and tornado-like vortex motion about the spinning cylinder. However, these observations were for an "annular" device with a very large gap size—essentially a spinning rod in a tank. Thus the flow behavior and free surface motion is substantially different from that seen for Taylor-Couette flow with a narrow gap.

Wardle and coworkers were the first to attempt to apply free-surface capturing CFD methods to simulate gas-liquid free surface flow in the centrifugal contactor mixing zone at relevant conditions [27, 141]. Using volume of fluid (VOF) methods [142] and the commercial code Fluent, the free-surface flow in a lab-scale centrifugal contactor having a 50.8 mm rotor was explored [141]. Conditions were chosen for a low-moderate flow rate at a typical rotation rate for this size device (377 rad/s). It was discovered that the free surface is a critical characteristic of the flow in the annular region, with the result that contact between the fluid and the spinning rotor was both discontinuous and intermittent (see Figure 7 with images taken from Wardle et al. [143]). Entrained bubble velocity measurements from LDV are reported. In addition, time autocorrelation of the velocity data provided a quantitative measure of the periodic free surface oscillation that was observed in both visually (high-speed video) and computationally. Excellent quantitative comparison was achieved for the frequency of oscillation. Elsewhere [144], the frequency and magnitude of oscillation is reported as a function of flow rate and rotor speed and was observed to decrease with an increase in either parameter. This same experimental study reports additional data for PIV-measured velocities at several flow rates and high-speed imaging of bubble entrainment under the rotor in the vane region for two vane types (4 straight vanes and 8 straight vanes).

In a follow-on study [27], the methodology was applied to explore numerically the effect of the mixing vanes (see Figure 8) on the annular liquid flow. As observed in companion experiments (see also [144], the predicted liquid hold-up volume and height was found to be a strong function of the vane configuration. Vane configurations with four straight vanes (4V), eight straight vanes (8V), and eight curved vanes (CV) were tested. It was seen that fewer vanes resulted in greater liquid volume, liquid height, and fluid-rotor contact due to reduced "pumping" by the housing vanes with the ranking in order being 4V > 8V > CV. A case with the addition of a gap between the vane and the outer wall and one with a narrower annular gap were also tested for the 8V case (additional images and analysis for these cases is reported in Wardle et al. [141]). It was found that the volume holdup (and consequently the residence time) could be increased by 54% by adding a vane-wall gap equal to half the annular gap. Comparison of mixing as characterized by the turbulent energy dissipation rate, which is directly correlated with droplet size for liquid-liquid systems, followed a similar trend. Despite the value of such relative comparisons, absolute prediction of the height of the liquid in the annulus and hold-up volume is difficult due to uncertainties in the boundary conditions at the rotor inlet; coupled solution of the two regions (annulus and rotor) can eliminate this problem and have recently been reported Wardle [145].

A significant challenge with free-surface modeling techniques is that they are inherently mesh dependent; only interfacial features that can be resolved on the mesh can be captured. As a further limitation, such methods are time dependent by nature and are limited by the Courant flow number:

$$\mathrm{Cr} = \frac{\Delta t}{\Delta x/\vec{u}} \approx 0.25. \tag{15}$$

Thus, the time step Δt is directly proportional to the mesh spacing Δx (u is the flow velocity)—that is if the mesh spacing is cut in half to increase interfacial resolution, the time step must essentially be decreased by the same margin. Consequently, such methods are quite computationally intensive when applied to large systems. A recent study by Wardle and Lee [146] explores the application of a computationally scalable technique using a finite element-based implementation of the lattice Boltzmann method to free surface flow in an annular mixer. While the methodology can be extended to turbulent flows, this study was limited to very low rotation rates and thus the effect of the free surface was small. Good comparison was found with the experimental results of Watanabe et al. [137] which explored a similar range of rotation speeds.

6. CFD Simulation of Single-Phase Flow in the Separator Zone

Patra et al. [147] have studied the hydrodynamics within the rotor using computational fluid dynamics with standard k-ε model. The rotor diameter has been varied over a wide range of 15 to 375 mm and the rotor speed 20 to 175 rad/s. A comparison has been presented between the CFD predictions and the experimental measurements reported in

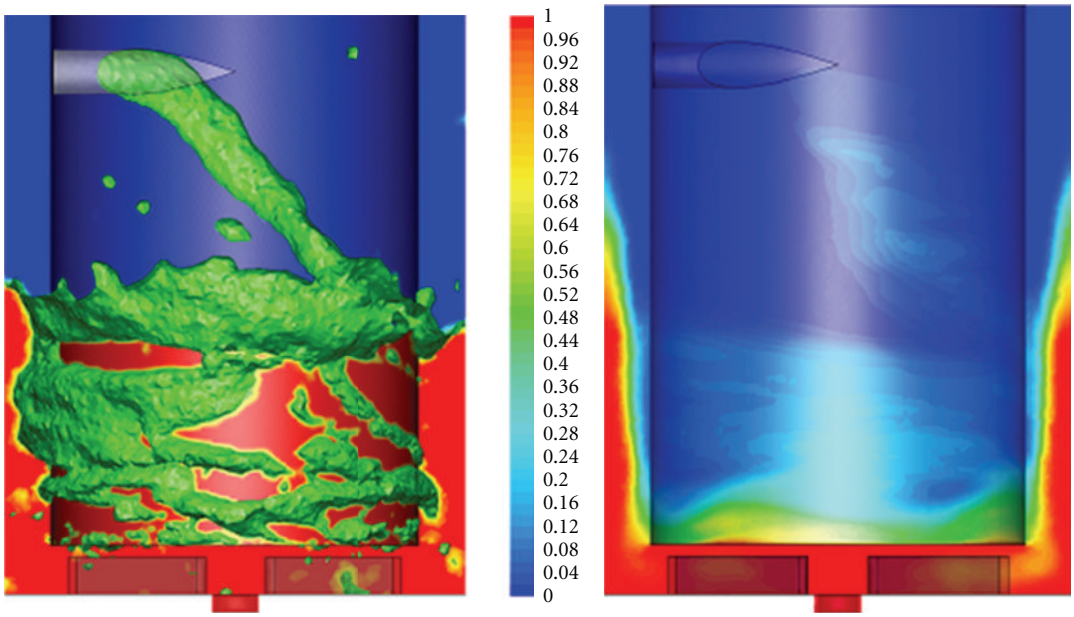

Figure 7: Snapshots of instantaneous (a) and time-averaged (b) liquid volume fraction for free-surface simulation of the annular mixing region with four straight housing vanes. Images are taken from Wardle et al. [143].

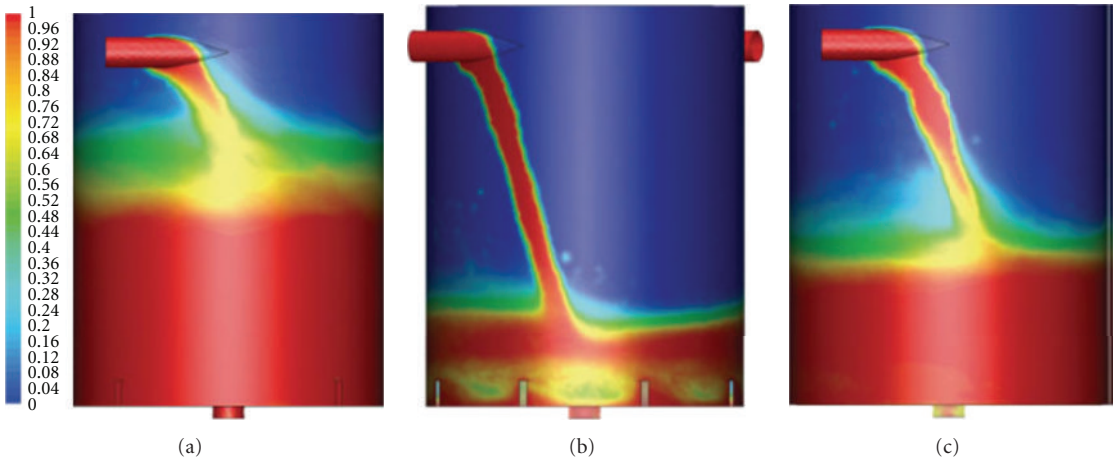

Figure 8: Time-averaged water volume fractions in the annular region from CFD for the 4-vane (a) 8-vane (b) and curved vane (c) geometries [27].

the published literature. The hydraulic performance of rotor as a centrifugal pump has been presented in terms of head, capacity and power consumption. The flow pattern in the suction and settling zones of the contactor has been presented with streamlines, static pressure distribution, and the velocity profiles.

The flow inside the rotor of ACE was found to be turbulent-forced vortex flow. The energy dissipation increased with an increase in the rotor speed. The CFD simulations satisfied the overall energy balance. The energy input rate by rotation was equal to the sum of the viscous and the turbulent energy dissipation rates. Such a balance was found to hold for all the rotational speeds and the rotor sizes. As a consequence of rotation, zone of negative pressure was created at the rotor inlet resulting into a suction of liquid at the bottom center and delivering it at the top of the bowl. The pumping rate was found to increase with an increase in the rotor speed. The throughput system also increased with speed of rotor. Additionally, the available static pressure was found to help in interstage pumping. With an increase in the diameter of the rotor, the pumping capacity of rotor was found to increase. With an increase in the inlet orifice diameter, the pumping capacity of the system was found to increase initially at a faster rate. Further increase in orifice diameter had a nominal effect at relatively low rotational speeds, however, sizeable effect at high rotational speeds.

The trajectory of fluid inside the rotor was observed to follow a spiral helical path originating from the rotor inlet and coming out at rotor outlet. The method of CFD simulation in the work by Patra et al. [147] is expected to be useful for the estimation of pumping capacity while designing these equipment in practice.

7. CFD Simulation of Two Phase Flows on the Annular Side

As with the contactor as a whole, the flows in the annular mixing region include both phase segregated and dispersed flow regimes—"clean" fluids enter a stage and flow as rivulets down the housing wall or, if the feed velocity is high and the annular gap small, impinge on the rotor and are thrown off as droplets. The shear induced in the narrow annular gap by the spinning inner cylinder causes the two fluids to mix to some extent with one phase becoming dispersed into the other and the size of the dispersed phase droplets depending on the fluid properties and flow conditions [148, 149]. Traditional CFD modeling such as that which has been done to date and described in the following sections is flow regime dependent—that is different methods are used for segregated, sharp-interface flows than are used for dispersed flows. Recent promising work has been reported by Wardle and Pereira [150] on the development of hybrid methods as an extension of the techniques demonstrated for Eulerian multifluid—VOF coupling given in Štrubelj et al. [151].

7.1. Liquid-Liquid Stratification. In a recent paper [145], Wardle presents an attempt to simulate the multiphase flow in the annular mixing zone using interface capturing techniques to resolve large droplets and liquid-liquid structures. A model annular mixing zone with four straight housing vanes was used. As stated in the paper, this effort was primarily to demonstrate the limitations of a VOF-only formulation and the need for development of advanced methods which combine dispersed phase modeling with sharp interface capturing. It was found that while the incoming fluid streams did indeed breakup into smaller chunks and droplets, the majority of each fluid remained as large rivulets as shown in Figure 9 reproduced from that work. An additional observation from these simulations is the fact that in relation to air, the two liquids tend to behave as a single fluid. It is thus concluded, that a sharp interface is only required between either liquid phase and air in order accurately capture the physics of the fluid-rotor interaction and in order to capture liquid-liquid mixing dispersed phase modeling could be employed. Yet, the combination of these two techniques is not currently available in any commercial CFD packages.

In this same work [145], extension of the same sharp-interface, three-phase methods to the entire contactor was also performed and the results demonstrated the well-known tendency of VOF methods to overpredict coalescence of droplets. Once the "mixed" liquid-liquid flow entered the rotor, the two fluids were seen to promptly separate. Despite these limitations of a VOF-only methodology, this work provides a foundation for further developments toward multiphase flow simulation and also demonstrated the applicability of the open-source package OpenFOAM to serve as the basic framework for future methods developments in this area.

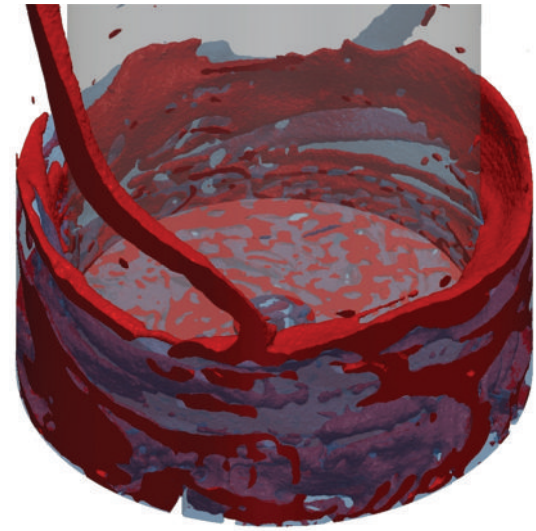

Figure 9: Snapshot of liquid phases for liquid-liquid-air simulation of a contactor mixing zone using VOF interface capturing methods taken from Wardle, [145]. Water is shown as transparent blue and oil is red while the air is not colored.

7.2. Liquid-Liquid Dispersion. Just as for the single-phase regime, simplification of the mixing zone flow to look only at liquid-full (no air or free surface), liquid-liquid dispersed flow in the annular region has been explored by several researchers due to its broader application to general two-phase Taylor-Couette flow devices. As such, the majority of work to date in this area has primarily been focused on application to low shear, laminar liquid-liquid extraction [152]. Campero and Vigil [29] have examined experimentally various flow patterns for liquid-liquid Taylor-Couette-Poiseuille flow (TC with added axial flow) for several different liquid-liquid phase pairs including water-kerosene for a horizontally oriented annular device. They looked at Reynolds numbers up to ~5000 and identified three flow regimes: (1) translating banded flow, (2) spatially homogeneous flow, and (3) oscillatory/alternating combination of (1) and (2) depending on the Weber and Reynolds numbers of the flow. This same experimental setup was used by Zhu and Vigil [153] for further study of the kerosene-water system for both experimental and numerical studies of liquid-liquid flow in a horizontally oriented Taylor-Couette device. Building on the previous work, they proposed a mechanism for the formation of banded liquid-liquid flow—alternating aqueous-rich and organic-rich vortices—which occurs for the upper end of the range of relatively low Re studied ($\mathrm{Re} = 300 \sim 5000$). A very useful recent study by Sathe and coworkers [28] explores a broader range of flow regimes both experimentally and computationally for

a vertically oriented Taylor-Couette mixer using a sodium iodide solution as the dispersed phase and kerosene as the continuous one. While no air- or air-liquid-free surface is present, a range of flow regimes spanning segregated to homogeneously dispersed liquid-liquid flows was explored. Data includes velocities and hold-up fraction from PIV and PLIF, respectively, and droplet size characterization using high-speed imaging. Droplet size measurements were made only for relatively low rotation rates where droplets sizes were in the range of 1-2 mm at a dispersed phase fraction of 0.5. PIV and PLIF were done for low rotation rates and dispersed phase fractions <0.1. Simulations were done over a wider range of conditions using Fluent with an Eulerian two-fluid model and a 2D, axisymmetric annular geometry. A fixed dispersed phase droplet diameter as predicted using the correlation by Haas [148] was imposed. CFD simulations were conducted up to rotation rates where the predicted droplet size was 30 microns and homogeneous dispersion resulted. While comparison between simulation and experiment was generally good, it was concluded that the assumption of a constant diameter droplet size required by the methodology resulted in some unavoidable deviations. The droplet size was additionally found to have a significant affect on the overall flow appearance.

7.3. Gas-Liquid Dispersion. Due to the annular region being "open" to air, in addition to the formation and rotation of the free surface, there is also air that is entrained as bubbles in both single liquid and liquid-liquid flow conditions. Various researchers have looked at the effect of air bubbles and their distribution in turbulent Taylor-Couette flow. Unlike what was seen for a lighter liquid dispersed in a heavier continuous phase where droplets tended to go toward the vortex cores, it has been shown that bubbles migrate toward the inner cylinder and are most stably located in rings along the regions of outflow between toroidal TC vortices [154–157]. Numerical studies have also been able to predict this behavior [154, 158, 159]. Batten et al. [160] developed a method of using the average bubble distribution to identify the location of Taylor cells. Additionally, one effect of the bubbles accumulation near the inner cylinder is the reduction of drag and corresponding decrease in energy dissipation [161]. This is important as energy dissipation is a key measure of the mixing intensity and is consequently directly correlated to droplet size for liquid-liquid mixing.

Atkhen et al. [154] have observed the fluid mechanics of an annular contactor apparatus with radial vanes beneath the rotor directing the flow toward a downward axial exit (see also [149, 162]). The device used in this work had a very long aspect ratio (total height relative to annular gap)—hydrodynamic observations were made with a liquid height of ~50 cm and annular gaps of 5 mm and 10 mm. Thus, for this system under the range of conditions explored, the effect of the free surface was limited to the formation and distribution of air bubbles throughout the annulus. It was observed that at the high end of the range of rotation speeds explored ($\mathrm{Ta} > 5 \times 10^4$) that spatial and temporal defects due to free surface agitation led to elimination of stable Taylor vortices. Note that this is approximately an order of magnitude lower than the transition to fully turbulent Taylor vortex flow and several orders of magnitude lower than the Taylor number in typical annular centrifugal contactor flow.

8. CFD Simulation of Two-Phase Flows in the Separator Zone Including the Overflow Weirs

8.1. Flow Simulation for Gas-Liquid System inside the Rotor. As described earlier and shown in the general contactor sketch in Figure 1, the flow of the liquid-liquid dispersion enters the spinning rotor and is thrown towards the outer wall where the two fluids separate as they flow upward. As the upper section and outlet channels are open to air, a vertical column of air (which would be more of a typical vortex at lower rotation rates) also develops along the axis of the rotor. Thus, even in the rotor a complex, three-phase system exists. Further, the flow of the separated liquid streams over their respective weirs occurs as a free-surface and may exist as droplets or rivulets depending on the magnitude of flow and operating conditions. Proper sizing of the heavy-phase and light-phase weirs and outlet channels is essential for achieving optimum throughput with no other phase carryover (unseparated dispersed phase which leaves the stage with the continuous phase and degrades overall extraction efficiency) for a given liquid-liquid system. While non-CFD approaches (described in Section 2.2) to modeling the operation of the rotor using hydrostatic balance arguments and various flow correlations [107, 163] have been successful at providing a useful means for proper weir design, relatively few CFD-based studies have been conducted to help understand the flow in this region of the contactor and aid in more fundamental design and operational optimizations.

Wardle et al. [143] applied the same free surface simulation methodology mentioned above in the context of the mixing zone to exploration of the flow of a single liquid phase in the rotor of a lab-scale contactor. The actual rotor geometry from a contactor manufactured by CINC Industries (CINC-V2) was used and the solution was done within a rotating reference frame. The authors demonstrated that at normal operating speeds the liquid forms a vertical annulus on the outer wall with a stable air column in the center. A methodology for predicting the zero-point flow rate (single-phase feed rate at which flow begins to exit from the light-phase side) using CFD was developed. In addition, interesting flow phenomena in the region above the heavy-phase weir was identified which helped to explain experimentally observed behavior—namely, elevated and sometimes unstable heavy-phase throughput [164]. It was discovered that the narrow flow region above the upper weir formed by a cap, which in this design holds the changeable weir in place, could potentially seal with liquid forming a siphon and artificially elevating the throughput through the heavy phase side (Figure 10(a)). Simulations and experiments verified that venting of the cap could eliminate this siphon formation.

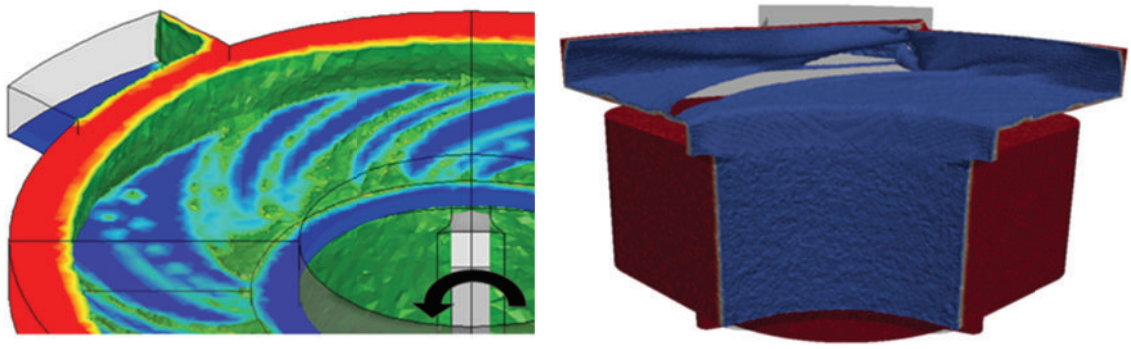

(a) (b)

Figure 10: (a) Snapshot of free surface flow over the upper weir at high flow rate showing liquid accumulation under weir cap [143], (b) Snapshot of free surface flow over the upper weir at high flow rate showing liquid accumulation under weir cap [165].

Building on the previous simulations for the full rotor, Gandhir and Wardle [165] explored the flow in the aqueous underflow region (region on heavy phase side above item 10B in Figure 1) and above the upper weir using free-surface capturing, this time using the open-source CFD toolkit OpenFOAM as the CFD package. While significant liquid accumulation and some negative pressure buildup was observed, complete liquid sealing of the weir cap outlets was not found in this case (Figure 10(b)) and was attributed to the greater mesh resolution used in this study relative to the earlier one. The relative pressure drop in the underflow region was investigated and found to vary only slightly with different modifications to the weir cap. While cap design modifications were proposed which can smooth the outlet flow, as with the previous work on the full rotor [143], it was determined that a cap vent is required to regulate pressure and ensure smooth and predictable operation as seen with an open upper weir.

Using the open-source CFD package OpenFOAM, Wardle also reported the first coupled-region model simulations for the combined annulus and rotor zones using multiple moving reference frames and sharp interface capturing for gas-liquid flow and gas-liquid-liquid flow [145]. Figure 11 taken from that work shows a snapshot of the liquid flow for the two-phase, water-air case for this couple-zone model. As noted in that work, a coupled-zone model eliminates the need for difficult approximations of boundary conditions at the rotor inlet which make it challenging to independently predict annular liquid height or its effect on rotor flow.

Figure 11: Simulation of free surface flow (water, air) in for a coupled annular mixer, rotor centrifugal contactor model taken from Wardle, [145]. The spiraling flow of liquid over the upper weir can be seen; rotor rotation is in the counter-clockwise direction.

8.2. Flow Simulation of a Liquid-Liquid System inside the Rotor. A 2006 study by Padial-Collins et al. [166] looked at the separation of a liquid-liquid mixture using an Eulerian multifluid framework (per-phase momentum equations for dispersed phase modeling of phases as interpenetrating continua). This work employed a simplified rotor geometry (2D and 3D) which was assumed to be entirely filled with the separating dispersion (no air core). For their dispersed phase modeling, the authors used a fixed dispersed phase diameter of 150 microns which reportedly mimicked the experimentally observed separation time. The influence of "effective" mixture viscosity, which is greater than that of either phase alone, was explored and found to be important to the separability of the two phases. Additionally, it was suggested that an outward sloping rotor interior sidewall could potentially increase the phase separation capacity of the rotor for a given throughput.

8.3. Effect of Annulus Liquid Height on the Flow Profile Inside the Separator. Liquid height in the annulus is critical to the optimized design and operation of the ACE. While the throughput of a given contactor is typically limited by the capacity for complete separation of the two phases within the rotor, such that there is minimal other-phase contamination in the respective outlets, another limiting case is the understanding if the dispersion in the annulus fills the mixing zone, and overflows into the organic collector ring. Even if the liquid height under nominal conditions is

acceptable, flow transients and changes in the liquid height due to phase inversion make the annular liquid height an important factor during operation.

9. Conclusions

(1) The annular region of the annular centrifugal extractor (ACE) has been simulated using computational Fluid Dynamics over a wide range of design and operating conditions, such as (Table 1): $22.2 < D_i < 500$ mm, $1.5 < d < 25$ mm, $1.67 < N < 60$ r/s. This covers the Taylor number range of $50 < \mathrm{Ta} < 3 \times 10^8$. In majority of the cases, single-phase flow has been simulated.

(2) For the simulation of annular region, k-ε, RSM and LES have been employed as turbulence models. Among k-ε and RSM, the latter has been found to give more reasonable predictions of three components of mean velocity, Reynolds stresses, k and ε. Extensive comparisons have been presented by Vedantam and Joshi [3],Wardle et al. [133], Deshmukh et al. [26, 132], and Deng et al. [123].

(3) Though LES has been employed by a few investigators, the grid size has been coarse.

(4) The CFD simulations give the value of turbulent energy dissipation rate (ε) at all the locations of simulation. The volume integral of ε gives the total energy dissipation in the simulation region. It has also been shown that the viscous dissipation is not negligible particularly in small scale equipment and where the velocity gradients are steep. The simulated energy dissipation rate needs to be equal to the energy supply rate by the impeller rotation. Such a complete energy balance has been established by Vedantam and Joshi [3], Deshmukh et al. [26, 132], Sathe et al. [28], and Tamhane et al. [105]. The establishment of such energy balance has been considered to be an important criterion for the validity of CFD simulation.

(5) Taylor [84] has experimentally measured the transition points from purely tangential flow to Taylor-Couette flow. These experiments were performed over a wide range of rotational speeds of inner and outer cylinders. The effects of corotation and counter-rotation have been examined. However, the gap between the cylinders was small. Therefore, Chandrasekhar [87] considered the case of large gaps and found the transition criterion analytically. Further, Rayleigh [83] has developed a criterion for inviscid fluids. For all these three cases of Taylor, Chandrasekhar and Rayleigh, the transition points can very well be predicted by the CFD simulations [26].

(6) The value of Ta at which the first transition occurs from Couette flow (CF) to Taylor vortex flow is designated as critical Taylor number ($\mathrm{Ta_{Cr}}$). For the stationary outer cylinder, as Ta increases beyond $\mathrm{Ta_{Cr}}$, the flow transition occurs to wavy vortex flow (WVF, $\mathrm{Ta_{Cr}} < \mathrm{Ta} < 100\ \mathrm{Ta_{Cr}}$), then to chaotic vortex flow (CVF, $100\ \mathrm{Ta_{Cr}} < \mathrm{Ta} < 1000\ \mathrm{Ta_{Cr}}$) and finally to turbulent Taylor vortex flow (TTVF, $\mathrm{Ta} > 1000\ \mathrm{Ta_{Cr}}$).

(7) The effects of operating parameters like rotor speed and axial flow rate on the number of Taylor vortices formed in the annular region have been observed by Deshmukh et al. [26, 132]. They showed that the number of Taylor vortices decreases with an increase in rotor speed. Also, when an axial flow was imposed on the existing rotational flow, the number of vortices decreases with an increase in the net axial flow.

(8) Deshmukh et al. [119, 132] and Tamhane et al. [105] have also studied the flow patterns in presence of helical baffles in the annular region. They observed that each compartment contained a pair of counter-rotating Taylor vortices. This fact was shown to aid an approach to plug flow behaviour.

(9) Deng et al. [123] have investigated the Taylor vortex flow in a short column in presence of vertical and horizontal baffles on the outer cylinder. The calculation resulted from CFD simulation agreed well with the PIV measurements. The introduction of vertical baffles eliminated the axisymmetric vortex structure and resulted in a three-dimensional flow pattern, including the circulation flow in the radial-azimuthal plane and the periodic variation of the vertical position of vortices. The horizontal baffle separated the original fluid column in compartments, and the length of the vortices inside was variable in a certain range to fit the compartment dimension. It was found that the number, position, and width of the baffles affected the vortex structure in the annulus. This study could provide informative insight to many engineering applications of Taylor vortex devices.

(10) The computational methodology of Wardle et al. [27] has been further validated and applied to perform a detailed analysis and comparison of the flow and mixing for several possible housing vane configurations. In general, it has been seen that the housing vane geometry has a significant impact on the overall flow patterns, liquid height and liquid volume, fluid-rotor contact, and energy dissipation rate in the rotor region.

(11) The presence of vanes on the bottom plate, below the rotor, essential to direct the flow inside the rotor has been shown to enhance the back-mixing and turbulence [132]. The CFD results show that providing suitable internals such as radial baffles as well as the length of vanes on the bottom plate can reduce backmixing in the annulus.

(12) Wardle et al. [133] presented the results of CFD calculations of the flow in the mixing region of an annular centrifugal contactor applying various simplifying assumptions (i.e., steady-state, liquid full contactor, and single liquid phase) and using relatively simple CFD models. It was found that realistic, qualitatively accurate results could be obtained for the flow underneath the rotor.

(13) Wardle et al. [141] have presented a comparison of experimental measurements and computational modeling of the free surface flow in the mixing zone of an annular centrifugal contactor. It was found that CFD modeling using the LES turbulence simulation method even for a relatively coarse computational grid was able to qualitatively and quantitatively predict the actual dynamics of the flow in the contactor mixing zone. A comparison with LDV data showed that the mean and RMS velocities were captured with much better accuracy by LES modeling than for either RANS or DES on the same mesh. Thus, for transient modeling of the flow in the contactor using the VOF interface-tracking method, it appears that greater accuracy can be obtained

from LES without a significant increase in computational cost. More importantly, this study has shown that the velocity predictions and free surface dynamics from CFD modeling of the centrifugal contactor are experimentally verifiable.

(14) A comparison presented by Wardle et al. [27] has shown both qualitatively and quantitatively that the mixing vane geometry has a clear impact on the overall effectiveness of the mixing zone. The conclusions obtained from the simulations were compared with a variety of experimental observations and found to have generally good predictive accuracy for the flow of water in the mixing zone. From this, it is anticipated that the experimental analysis and modeling scheme set forth here can aid in the proper selection of contactor geometry as well as lend insight into ways to improve the design of existing contactor units with minimal modification. In particular, from this comparison, it can be concluded that among the given configurations, one might select the 4-vane geometry for better low flow rate operation as it maintains a predictable liquid volume with greater fluid-rotor contact; however, at high flow rates (1000 mL/min), the liquid level is such that nearly the entire mixing zone is filled and there is the risk of overflow into the lower phase collector ring and phase contamination. This marks a practical upper limit for this geometry. While high flow rates were not simulated, it has generally been observed that adequate operation can be achieved with either the curved vanes or 8-vanes at high flow rates. For some processes and phase pairs, there may be issues with overmixing and emulsification. In such cases, this type of analysis could certainly aid in selecting an appropriate geometry and targeting experiments for improving operation for the flow conditions specified by the process. It has also been demonstrated that a noticeable improvement, both in terms of mixing and residence time, can be achieved through the simple addition to the standard 8 vane geometry of a vane-wall gap with a width equal to half the annular gap (d).

(15) The flow in the separation zone of the annular centrifugal contactor has been explored [143] through the application of detailed computational flow simulations of the actual geometry of a model rotor of a CINC V-2 centrifugal contactor. It was found that there is indeed a vertical column of air that develops along the axis of the spinning rotor. For moderate flow rates, the heavy phase exit ports above the upper weir remain open and there is droplet flow over the weir. At high flow rates, the flow area above the upper weir becomes sealed with water and forms a siphon which increases the amount of flow that can pass over the upper weir. This was observed quantitatively through prediction of the zero-point flow rate for the standard sealed upper weir cap and for one with venting. Similar trends between the two weir caps were also observed experimentally. This research effort has viewed the contactor from the perspective of solvent extraction and has, therefore, deemed the zero-point elevation an undesirable quality. For operation of the contactor primarily as a dedicated separation device, it might be argued that a higher heavy phase throughput is advantageous. Even so, it can generally be concluded that a predictable throughput is preferable regardless of the application of the unit.

(16) The simulations by Wardle et al. [143] provide a detailed view of the flow structures within the rotor of the centrifugal contactor. In particular, specific details of the flow above the upper weir have helped to explain previously observed behaviors for this design of contactor rotors. As this commercial contactor design has been in general favorably evaluated for solvent extraction use by a number of studies [164, 167–169] the research presented here provides a tool for evaluating the design as well as a method for enabling greater general understanding of the flow and hydraulic operation of the separation zone of the annular centrifugal contactor.

(17) The CFD toolkit OpenFOAM was used by Wardle [145] to explore previously unreachable simulation space for multiphase flow in a model annular centrifugal contactor. In particular, liquid-liquid mixing simulations with a greater mesh refinement than the mesh number which was used earlier were performed. More importantly, mixing zone-separation zone were coupled. This package provides the necessary framework for developing advanced multiphase solvers specifically tailored to the physics of the problem at hand based on the limitations of existing methodologies as identified here. It is clear from these simulations that while the VOF methodology is capable of providing a general idea of the flow in both regions of the contactor, only underresolved simulations are possible because the mesh required for full resolution of the interphase mixing and resulting small droplets is computationally prohibitive even with massive HPC systems due to the fine meshing and very small time steps that are required.

(18) Wardle [145] have recommended that an interpenetrating (Eulerian-Eulerian), statistical multiphase modeling methodology coupled with VOF for the liquid-air interface(s) be employed to enable prediction of the physical effects of the unresolved droplet scales. Additional coupling of such a solver with droplet size distribution information is expected to a simulation framework capable of providing unique insight into the area of solvent extraction process simulation in a variety of process liquid-liquid contacting equipment including the annular centrifugal contactor.

(19) Zhu and Vigil [153] have investigated that banded distributions of disperse-phase droplets are characteristic of liquid-liquid Taylor-Couette flow with a fixed outer cylinder. These structures arise when centrifugal forces associated with the rotation of the vortices themselves, as opposed to the inner cylinder, are sufficiently strong to cause droplet migration to vortex cores ($\rho_p < \rho_C$) or to vortex inflow boundaries ($\rho_p > \rho_C$). For the case of a less dense disperse phase, the scaling relation provided by (6) (in their paper) appears to correctly predict the "bandedness" of liquid-liquid Taylor-Couette flow. However, its usefulness as a predictive tool is limited by the lack of prior knowledge concerning (1) the azimuthal velocity component u_θ, with respect to the vortex rotational axis in the core on the outer layer of a vortex, and (2) the turbulent viscosity in the vortex cores. Droplet diameters can be estimated by using Haas's correlation, (2) [148]. As a first approximation, for small particle loadings one would expect u_θ to be independent of α

and d_P and to be proportional to the inner cylinder angular velocity so that $u_\theta/\Omega_i R_i$ = constant.

Authors have also suggested that, a plot of this ratio against azimuthal Reynolds number results in

$$\frac{u_\theta}{\Omega_i R_i} = 0.14. \tag{16}$$

Calculation of the mixture turbulent viscosity at the vortex core is more difficult, as this quantity depends upon the local turbulent kinetic energy and turbulent dissipation, which in turn are composition-dependent quantities. Equation (6) is strongly dependent on the mean droplet diameter, which in turn depends more sensitively on We than on Re, according to (2) (Both equations from Zhu and Vigil [153]). A decrease in interfacial surface tension through the introduction of a surfactant, therefore, is a more effective means for reducing droplet size than is a proportional increase in the angular velocity of the inner cylinder. For fixed interfacial surface tension, experiments and FLUENT simulations show that the disperse phase becomes progressively more homogeneously distributed as the azimuthal Reynolds number is increased.

(20) An experimental facility for measuring orthokinetic aggregation has been developed by Wang et al. [170] and tested. By making use of a CCD camera and an in-line optical assembly, nonintrusive measurements of particle size distributions have been performed. The evolution of a surfactant-free polystyrene sphere aggregation process under various mean shear rates in the laminar Taylor vortex flow regime has been investigated.

The authors have made the following additional observations.

(i) The mean aggregate particle size, d_{43}, grows before reaching a steady-state value, which depends upon the value of the mean shear. Specifically, the steady-state value of d_{43} decreases with increasing shear rate, which suggests that aggregate breakup is the reason that particle growth ceases. Further evidence of this is provided by the fact that the steady-state value of d_{43} is independent of the total initial monomer concentration. In contrast, if the cessation of particle growth was due only to the presence of too few particles rather than to breakup of aggregates, one would expect the steady-state value of d_{43} to depend on the total initial monomer concentration. (ii) The two-dimensional perimeter based fractal dimension of the flocs, D_{pf}, was used to quantify aggregate structure. A comparison of time plots of the mean particle size d_{43} and D_{pf} shows that initially aggregates have a ramified, open structure that becomes more compact as breakup-induced restructuring occurs even after the mean aggregate size has reached steady state. Such restructuring is consistent with the observations of other investigators. (iii) Although the experiments described here were performed in a batch mode because of the slow growth of aggregates, the Taylor-Couette reactor could prove to be convenient for studying faster aggregation processes. In particular, by operating the Taylor-Couette reactor in a steady-state continuous mode so that a weak axial flow causes axial translation of the Taylor vortices with minimal disruption, optical PSD measurements can be obtained at leisure at various axial locations in the reactor. (iv) If the reactor is operated in the laminar Taylor vortex regime, each axial location will sample particles with identical residence times. Such measurements are impossible with other common continuous flow devices, such as stirred tank reactors. Velocity field measurements obtained by PIV were used to validate the CFD model implemented on Fluent. Thus the shear field can be obtained accurately for the simulation of aggregation and breakage. The simulation of particle size enlargement can be done by using average shear, and it can provide useful information about the parameters in the model. However, use of CFD is necessary for accurate simulation of simultaneous aggregation and breakage processes, especially when reactions occur on short time scales.

(21) Padial-Collins et al., [166] have solved the momentum and mass conservation equations in the simulation of the separation of the aqueous and the organic components in the rotor zone of a centrifugal contactor. The authors have demonstrated a computational scheme and a tool which can be used to examine complex hydraulics, to explore effects of the geometry in the process, and to study the influence of different initial conditions, distinct rotor speeds, and diverse physical contributions. We have studied the importance of the effective viscosity. Its effect seems important at the low and high angular velocities, especially for the vertical contactor case. Since the objective is to reach very high extraction efficiency, the more accuracy in the modeling of effective viscosity in the simulations may be necessary. The calculations also show a potentially strong effect from mass transfer on the dynamics, indicating the need for realistic mass transfer parameters before more definitive statements can be made. Ultimately, these simulations aim at improving the efficiency of the centrifugal contactors by allowing, for example, investigation of alternative shapes for the devices or suggesting more appropriate initial conditions. Both of these had significant effects in our simulations. Future plans include the evaluation and optimization of advanced designs for contactors as well the investigation of the issue of scale to determine the minimum size for pilot units.

(22) The dispersion in a vertical Taylor-Couette contactor has been studied by Sathe et al. [28] experimentally as well as computationally. The experiments have been also carried out using high-speed imaging for getting the information about the drop sizes. The correlation by Hass was found to give comparable estimate of the drop sizes. The slight deviation observed was due to the dependence of holdup on the drop size in the annulus. The correlation by Hass does not contain the holdup of the dispersed phase, whereas the actual drop size depends on it. For this reason, the correlation seems to predict the drop size well at low-dispersed phase holdup values in the annular region.

(23) The PIV measurements have also been carried out [28] for the single-phase flow. A very good agreement has been found between the CFD predictions and experimental data in terms of mean velocity profiles as well as the number of vortices. The CFD simulations for the single-phase flow and also with multiphase flow have a limiting case of $\epsilon_D = 0$. The PIV images were processed to obtain the velocity vectors

under the similar conditions. It was found that the number of vortices and the spacing between them obtained with the PIV were in good agreement with those shown by the CFD simulations.

(24) Simultaneous measurements of flow field and dispersed phase holdup have been performed by Sathe et al. [28] using PIV and PLIF techniques, respectively. The experimental data were used to validate the CFD simulation. A good agreement has been observed for the mean velocities, number of vortices, and hold-up profiles within the acceptable limits. It was also observed that the results obtained with single-phase CFD simulations matched with those obtained with the simulations using the Eulerian multiphase model with $\epsilon_D = 0$. Thus, it was concluded that Eulerian multiphase model could be extrapolated to single-phase model when the holdup of the dispersed phase is taken as zero.

(25) The effect of physical properties like density difference and interfacial tension and the effect of geometrical parameters such as annular gap on the flow patterns have been studied by Sathe et al. [28] using CFD. The results have been represented in the form of regime maps with the Eotvos and Taylor number as the two coordinates. The results are independent of dispersed-phase hold-up for $\epsilon_D > 0.05$.

(26) At very low rotational speeds ($\mathrm{Ta} > 2 \times 10^6$, $\mathrm{Eo} < 0.046$), Sathe et al. [28] have shown that the two phases remain vertically stratified with a clear interface in between them. Further, these authors have shown that, at moderate rotational speeds, segregated flow can be observed when, $\mathrm{Eo} > 0.046$, and $7 \times 10^6 > \mathrm{Ta} > 2 \times 10^6$ or $\mathrm{Eo} > [1.87 \times 10^{-7}\,\mathrm{Ta} - 1.26]$, $\mathrm{Ta} > 7 \times 10^6$. In such cases the light phase gets dispersed in the heavier phase at the bottom as well as heavy phase is observed to be dispersed in the light phase at the top.

(27) Sathe et al. [28] have shown that, when the drops are large, centrifugal force on the drops due to tangential rotation of fluid around the cylinder axis was found to be dominant which gives a banded dispersion such that $\mathrm{Ta} > 7 \times 10^6$ and $\mathrm{Eo} < [1.87 \times 10^{-7}\,\mathrm{Ta} - 1.26]$ (for $\mathrm{Eo} > 0.046$) or $\mathrm{Eo} > 5.04 \times 10^{-2} - 6.23 \times 10^{-11}\,\mathrm{Ta}$ (for $\mathrm{Eo} < 0.046$). The dispersed phase in this case was found to mainly accumulate near either outflow or inflow region of Taylor vortices for $\rho_C > \rho_D$ or $\rho_C < \rho_D$, respectively. Also, when the drops are small and/or the density difference between the phases is small homogeneous dispersion can be observed, such that $2 \times 10^6 < \mathrm{Ta} < 7 \times 10^6$, $\mathrm{Eo} < 0.046$ or $\mathrm{Ta} > 7 \times 10^6$, and $\mathrm{Eo} < [5.04 \times 10^{-2} - 6.23 \times 10^{-11}\,\mathrm{Ta}]$.

(28) A systematic investigation by Gandhir and Wardle [165] has shown that the design of the weir cap has a significant effect on the flow patterns above the weir as well as on the pressures generated in this region. In turn, the pressure drop will have an influence on the throughput as characterized by the zero point flow rate. A number of variations and modifications to the weir cap design were simulated and, combined with insight from the previous work. The authors have made a number of recommendations. These simulations all considered only for the CINC-V2 contactor design. While no relevant data has been published, it appears from available information from preliminary tests at Argonne and elsewhere that the larger CINC units such as the V5 and V10 are equally effective if not more susceptible to negative pressure effects and siphon formation in the cap region and, therefore, the conclusions here should be equally applicable to those units. Measurements of the relative dimensions of the weir cap for the CINC-V5 contactor show that the heavy-phase outlet channel is much longer, with an aspect ratio of 1.25 compared to only 0.45 for the V2. This, in addition to minor underscaling of the channel width and the gap space above the weir, may indeed be the cause of the observed propensity for negative pressure effects and siphon formation.

Simulations are underway with a V2 cap scaled to the V5 relative dimensions to confirm this hypothesis and the overall effects of these differences on the flow profile and siphon susceptibility. The following work elements are progressive.

(i) Recommendation (b) assumes that the recommendation (a) is complete and are aimed at modifications to existing contactor units in terms of (a) vent in the weir cap (with 2 or more holes), (b) orient the cap with the outlet channel aligned with the light phase outlet channel, (c) modify the cap according to design (b).

(ii) If recommendation (a) is implemented, (b) requires no additional effort to also implement. Item (c) requires some additional machining of the weir cap but should correspondingly offer some measure of additional stability of flow through smoothing of the exit flow profile. Additional simulations and experiments for the recommended modifications in the larger CINC contactor units (V5 and V10) should be done to verify that these changes have the desired effect.

(29) Tamhane et al. [57] have carried out drop size measurement studies with the help of phase Doppler particle analyser (PDPA). A wide range of power consumption was employed in these studies. The measurements were taken at two different hold up values, namely 2.5% and 7.5%. It was found that, the mean drop size decreased with an increase in the power consumption in the annulus. The decrease in drop size was sharp in the initial stages while it was gradual in the latter part.

(30) Tamhane et al. [105] also observed that the drop sizes increased with increasing hold-up values of dispersed phase. In order to compare the experimental observations with the analytical solutions, Rosin-Rammler distribution function is used. Moreover, the effect of drop size on Weber number was studied. It was found that the exponent of Weber number is around −0.58.

(31) A correlation for the drop diameter in the annular region of Annular centrifugal extractor has been proposed by Tamhane et al. [105], which takes into account the effect of operating parameters like fluid properties, power per unit volume, and hold-up. The correlation is based on their own measurements and all the results on drop size (in ACE) available in the published literature.

10. Suggestions for Future Work

(1) The subject of centrifugal instability has been discussed in Section 2.1. It consists of transition from purely circumferential flow to Taylor vortex flow. The subsequent transitions to (a) Couette flow ($Ta = Ta_{Cr}$), (b) wavy vortex flow (WVF) ($Ta_{Cr} < Ta < 100\,Ta_{Cr}$), (c) then to chaotic vortex flow (CVF, $100\,Ta_{Cr} < Ta < 1000\,Ta_{Cr}$) and finally (d) to turbulent Taylor vortex flow (TTVF, $Ta > 1000\,Ta_{Cr}$) were also described. However, the published work has been almost confined to single phase Newtonian fluids, small Taylor-Couette geometries with infinite length. The work needs to be extended to the practical cases of annular centrifugal extractors (ACEs) having gas-liquid interface at one end and the bottom baffled portion (Figure 1 (part 6)) at the other end. The work also needs to be extended to large size ACEs upto 1.5 m rotor diameter and 3 m rotor height. The work also needs to be extended to multistage counter-current ACEs.

As mentioned earlier, the reported work has been largely for single phase Newtonian fluids. The cases of liquid-liquid and gas-liquid dispersions together with a wide range of physical properties ($\rho_C, \rho_D, \mu_C, \mu_D, \sigma$, and nonNewtonian nature) need attention in future.

(2) The overall flow structures and axial mixing can be reasonably estimated by making a pseudohomogenous assumption to represent liquid-liquid dispersion. The first cut solution may be obtained by even ignoring the free surface and simply using single phase flow simulations. These single phase simulations will provide useful estimates of energy dissipation rates as well as axial mixing in the annular region. The estimates of energy dissipation rates may be then used to estimate representative droplet diameter to estimate mass transfer coefficients. The Eulerian-Eulerian (EE) approach can then be used to understand possible influence of slip between two liquid phases. Please note that more often than not effective drag in liquid-liquid dispersions will be a strong function of Kolmogorov length scale (energy dissipation rate). Appropriate correlations of effective drag coefficients should, therefore, be used while developing EE-based CFD models for ACE. These models can then be combined with volume of fluid (VOF) approach to capture free surface as well as possible entrainment of gas phase. This last approach invariably required 3D simulations and, therefore, is very compute intensive.

(3) The key design aspect of the bottom region is to provide appropriate resistance to flow from annular region to inner rotating cylinder. This is realized by providing baffles (fixed in number, shape, size, and location for a given configuration of ACE) as well as additional moving components to realize ability to manipulate resistance during the ACE operation (position of these can be modified to realize better operating conditions in ACE). Since the key design issue is to estimate flow resistance or pressure drop offered by the bottom region, single-phase CFD simulations using the pseudohomogenous fluid (representing liquid-liquid dispersion) are adequate. The choice of turbulence models (since the geometry is quite complex) and use of adequate number of computational cells are crucial to obtain accurate estimate of flow resistance and key features of flow in the bottom region of ACE. Such CFD models can be used to evolve appropriate guidelines for manipulating flow characteristics of ACE by influencing flow in the bottom region of ACE.

(4) In liquid-liquid stratification studies, the two-phase flow is another variation of a single-phase flow that explores the effect of interface on the vortex flow. A significant challenge with free-surface modeling techniques is that they are inherently mesh dependent; only interfacial features that can be resolved on the mesh can be captured. As a further limitation, such methods are time dependent by nature and are limited by the Courant flow number, in turn, showing the dependency of time step on mesh spacing. The regime transition is inherently a complex problem. The existing VOF based approach may, however, be used to obtain broad estimates of height required for realizing stratified layers. A combination of EE and VOF will be useful to simulate the flow in the inner rotor region of ACE. Closely linked with the flow characteristics of the inner rotor, the flow in the outlets and associated weirs is equally crucial to understand for realizing stable operation of ACE.

(5) The pressure drop across outlet weirs influences number of design parameters of ACE. CFD-based studies help in understanding the flow in the weir region and therefore several other key design parameters of ACE. Until recently, CFD modeling techniques had not been applied to the rotor design in ACE. However, a useful analytical approach was demonstrated for determining the proper dimensions of the weirs based primarily on experimental correlations and hydrostatic balance arguments [107]. While this method has been generally quite successful for rotor sizing of contactors with an open upper weir (and the obsolete air-controlled upper weir), some experiments with "closed" upper weir systems have produced behavior which cannot fully be explained by the existing theoretical models. One such unexplained behavior is the elevated throughput that has been observed for large upper weir sizes in these units. This same behavior has also been observed in larger units of this design. VOF approach or even a single phase approach may be used to estimate pressure drop across outlet weirs of ACE. CFD modeling can provide useful insights in resolving such issues.

(6) Better understanding of the flow within the rotor and specifically the flow over the weirs requires full simulation of the complex rotor and weir geometries and analysis of the liquid free surface flow. Further, such hydraulic simulations can calculate important flow quantities which characterize the rotor and weirs such as the zero-point flow rate. Zero-point flow rate refers to the point wherein, due to excess flow rate coming into the rotor, the liquid volume maintained in the rotor increases so much that the liquid starts to come out of exit ports without getting separated. These kinds of studies are barely reported in a couple of papers until date. In practice, the zero-point flow rate is used to verify fabrication consistency of a set of rotors with the same specifications, such as might be used in a multistage bank of contactors.

(7) The quality of simulated results using CFD models of course also crucially depends on numerical implementation

of selected model equations. Table 2 gives a summary of key numerical parameters (like the number of grids used, method of discretization, and the solution procedure) used by various investigators. It is essential that adequately fine mesh (compared to relevant space scales of the considered ACE) is used along with the higher order discretization schemes. The published CFD results are reviewed in the following sections in light of this brief review on formulation and solution of CFD models.

(8) The suggestions (2) to (7) above in terms of CFD simulations need to cover a wide range of geometries such as $30 < D_i < 1500$ mm, $30 < H < 3000$ mm, $3 < d < 100$ mm. Various baffle designs [105, 119, 123] need to be analysed for reducing axial mixing. For all these geometrical cases, a wide range of physical properties ($\rho_C, \rho_D, \mu_C, \mu_D, \sigma$, and nonNewtonian nature) need to be studied.

(9) The simulation of rotor (separator region) has received scant attention in the past. The future work may be undertaken in the following steps: (a) pumping capacity of the rotor for single liquid phase without any internals, however over a wide range of rotor diameter and height, bottom orifice diameter and the rotor speed, (b) the work can be extended for the case of internals such as diversion plate and baffles and also the details pertaining to the outlet weirs. (c) In the third step, the existence of gas phase can be considered in the central core region. (d) Simulations are needed for the separation of liquid-liquid dispersion into clean individual phases.

(10) It has been brought out in Section 3 that the Kolmogorov length scale in the mixing zone is of the order of 1 to 10 microns. This range is order of magnitude smaller than the classical process equipment such as stirred tanks, bubble columns, fluidized beds, packed columns, plate columns, among others. Therefore, any future efforts of large eddy simulation need to take into account this small range of Kolmogorov length scale. The LES is known to predict the hydrodynamic parameters more accurately than the RANS, k-ε, and RSM models. The LES simulations also give information on turbulent structures in terms of their size, shape, velocity, and energy distributions [64, 171–180]. These structures properties can then be related to the mechanisms of heat, mass, and momentum transfer [70, 73, 181, 182].

(11) The mixing and the separation zones contain liquid-liquid dispersions with possibly a drop size distribution. A population balance approach may be combined with CFD (for instance, [55, 183, 184]).

(12) The performances of mixing and separation zones are strongly interlinked. The rotor height (H) and rotor speed (N) are selected for clean separation. The values H, N, D_i, do decide the pumping capacity which also depends upon the level in the mixing zone.

(13) Accurate prediction of stage extraction efficiency can allow optimization of operation and design as well as identification of issues which lead to poor extraction efficiency. Prediction of stage efficiency requires an accurate prediction of specific interfacial area as well as interphase mass transfer coefficients. Prediction of interfacial area is a nontrivial challenge as it requires accurate models for droplet size variation and some method for capturing droplet size distribution (e.g., population balance modeling, interfacial area transport, etc.). While much can be drawn from similar efforts in the broader liquid-liquid mixing community, research evaluations of the many available correlations for droplet breakup and coalescence should be evaluated for applicability to annular contactors.

(14) While one key advantage of centrifugal contactors is their relatively short residence time and high throughput, for kinetically limited, processes this can be a drawback which necessitates use of a less efficient equipment type that can accommodate the required residence times. CFD-based design tools for design modifications aimed at increasing residence time in annular centrifugal contactors could be of great value for broadening the range of processes which can be successfully implemented using this technology.

(15) Computational work to date has primarily focused on the development of methods and models and their validation for controlled conditions in simplified geometries. Aside from a few specific efforts (e.g., [27]), little has been published on CFD-based efforts to explore the broad range of specific design elements (e.g., annular gap size, vane-rotor gap, etc.) though experimental observations have given some insight into several key features.

(16) As the rotor of the contactor is essentially a centrifuge, particulates can be problematic (even with filtering of feed streams) for long-term operation of certain processes and require periodic shutdown and cleaning of rotors. While shutdown and restart of contactors are easily and quickly accomplished and "clean in place" rotor designs are available [185], CFD tools offer a direct method of exploring particulate flow and evaluating operational limits and design and/or operational changes to mitigate particulate issues.

(17) This is a very challenging problem for computational modeling (and experimentation). However, it is known that the extraction efficiency for processes can be quite different depending on which phase is dispersed. Additionally, process upsets which lead to phase inversion can be problematic—particularly for very small contactors.

(18) Centrifugal contactors have been constructed over a very wide range of rotor sizes from 1 cm to many 10 s of centimeters [186]. Often very small contactors are used for process development and it is not always well understood how certain hydrodynamic effects (e.g., surface tension) differ between the various scales.

Notation

a: Acceleration (gravitational or centrifugal, m/s^2)
C/D: Flow rate ratio of continuous to dispersed phase (–)
Cr: Courant number, Cr $= \Delta t/(\Delta x/\vec{u})$ (–)
d: Annular gap (m)
d_{43}: Mean aggregate particle size (m)
D_i: Diameter of rotor (m)
D_o: Diameter of stator (m)
D_{pf}: Two-dimensional perimeter-based fractal dimension of the flocs (m)

r_oEo: Eotvos number, Eo $= \Delta\rho g d_d^2/\sigma$ (–)
g: Acceleration due to gravity (m/s^2)
H: Height of the annulus (m)
N: Rotor speed (r/s)
N_D: Dispersion number (–)
Q: Volumetric flow rate of both phases through the settler (m^3/s)
r: Radial position from the rotation axis (m)
$\bar{r}$: Average radius of the dispersion band in ACE (m)
r_o: Radius of the inner edge of the dispersion band (m)
r_u: Radius of the outer edge of the dispersion band (m)
Re: Reynolds number of rotor, Re $= Ri\Omega_i^2 d/\nu^2$ (–)
Re$_Z$: Axial Reynolds number (–)
R_i: Radius of rotor (m)
t_B: Batch settling time of the dispersion (s)
t_R: Residence time of the dispersion in settler (s)
Δt: Time step (s)
Ta: Taylor number, Ta $= 4\Omega_i^2 d^4(\vartheta - \eta^2)/\nu^2(\eta^2 - 1)$(–)
Ta$_{Cr}$: Critical value of Taylor number, (–)
T_S: Settling time (s)
$\vec{u}$: Flow velocity (m/s)
u_r: Radial velocity (m/s)
u_θ: Tangential component of fluid velocity (m/s)
V: Volume of the dispersion band in the settling zone (m^3)
V_S: Settling velocity (m/s)
We: Weber number (–)
Δx: Mesh spacing (m)
ΔZ: Thickness of dispersion band (m).

Greek Symbols

ϑ: Rotational speed ratio of inner cylinder to outer cylinder (–)
ν: Kinematic viscosity (m^2/s)
ν_t: Turbulent kinematic viscosity (m^2/s)
η: Radius ratio, R_o/R_i (–)
μ_C: Viscosity of continuous phase (Pa.s)
μ_D: Viscosity of dispersed phase (Pa.s)
ρ_C: Density of continuous phase (kg/m^3)
ρ_D: Density of dispersed phase (kg/m^3)
ρ_p: Density of droplets (kg/m^3)
$\Delta\rho$: Density difference (kg/m^3)
σ: Interfacial tension between continuous and dispersed phase (N/m)
σ_ε: Turbulent Prandtl number for energy dissipation rate (–)
σ_k: Turbulent Prandtl number for kinetic energy (–)
ω: Angular velocity (rad/s)
ϵ_D: Volume fraction of dispersed phase (–)
ε: Turbulent energy dissipation rate per unit mass (m^2/s^3)
σ_ε: Turbulent Prandtl number for energy dissipation rate (–)
σ_t: Turbulent Prandtl number for kinetic energy (–)
τ: Reynolds stress (Pa)
Ω_i: Rotor speed (r/s).

Subscript

C: Continuous phase
D: Dispersed phase
i: Property pertaining to inner cylinder.

References

[1] D. S. Webster, A. S. Jennings, A. A. Kishbaugh, and H. K. Bethmann, "Performance of centrifugal mixer-settler in the reprocessing of nuclear fuel," in *Recent Advances in Reprocessing of Irradiated Fuel, Nuclear Engineering—Part XX*, W. A. Rodger and D. E. Ferguson, Eds., vol. 65 of *Chemical Engineering Progress Symposium Series*, no. 94, pp. 70–77, American Institute of Chemical Engineers, NewYork, NY, USA, 1969.

[2] G. J. Bernstein, D. E. Grosvenor, J. F. Lenc, and N. M. Levitz, ANL-7698, 1973.

[3] S. Vedantam and J. B. Joshi, "Annular centrifugal contactors—a review," *Chemical Engineering Research and Design*, vol. 84, no. 7, pp. 522–542, 2006.

[4] S. Vedantam, J. B. Joshi, and S. B. Koganti, "Three-dimensional CFD simulation of stratified two-fluid Taylor-Couette flow," *The Canadian Journal of Chemical Engineering*, vol. 84, no. 3, pp. 279–288, 2006.

[5] S. Vedantam, J. B. Joshi, and S. B. Koganti, "CFD simulation of RTD and mixing in the annular region of a Taylor-Couette contactor," *Industrial & Engineering Chemistry Research*, vol. 45, no. 18, pp. 6360–6367, 2006.

[6] B. D. Kadam, J. B. Joshi, S. B. Koganti, and R. N. Patil, "Hydrodynamic and mass transfer characteristics of annular centrifugal extractors," *Chemical Engineering Research and Design*, vol. 86, no. 3, pp. 233–244, 2008.

[7] B. D. Kadam, J. B. Joshi, S. B. Koganti, and R. N. Patil, "Dispersed phase hold-up, effective interfacial area and Sauter mean drop diameter in annular centrifugal extractors," *Chemical Engineering Research and Design*, vol. 87, no. 10, pp. 1379–1389, 2009.

[8] C. S. Schlea, H. E. Henry, M. R. Caverly, and W. J. Jekins, "Purex process performance with short-residence contactors," USAEC Report DP-809, 1963.

[9] B. F. Roth, "Centrifugal extractors for the reprocessing of nuclear fuels with high burn up and plutonium content," Tech. Rep. KFK-862, 1969.

[10] J. B. Joshi, C. B. Elias, and M. S. Patole, "Role of hydrodynamic shear in the cultivation of animal, plant and microbial cells," *Chemical Engineering Journal and the Biochemical Engineering Journal*, vol. 62, no. 2, pp. 121–141, 1996.

[11] Y. M. D. Tsao, E. Boyd, G. J. Spaulding, and D. A. Wolf, "Fluid dynamics within a rotating bioreactor in space and earth environments," *Journal of Spacecraft and Rockets*, vol. 31, no. 6, pp. 937–943, 1994.

[12] T. Imamura, K. Saito, and S. A. Ishikura, "New approach to continuous emulsion polymerization," *Polymer International*, vol. 30, no. 2, pp. 203–206, 1993.

[13] K. Kataoka, N. Ohmura, M. Kouzu, Y. Simamura, and M. Okubo, "Emulsion polymerization of styrene in a continuous Taylor vortex flow reactor," *Chemical Engineering Science*, vol. 50, no. 9, pp. 1409–1416, 1995.

[14] J. B. Joshi, M. M. Sharma, Y. T. Shah, C. P. P. Singh, M. Ally, and G. E. Klinzing, "Heat transfer in multiphase contactors," *Chemical Engineering Communications*, vol. 6, no. 4-5, pp. 257–271, 1980.

[15] A. B. Pandit and J. B. Joshi, "Mixing in mechanically agitated gas-liquid contactors, bubble columns and modified bubble columns," *Chemical Engineering Science*, vol. 38, no. 8, pp. 1189–1215, 1983.

[16] A. B. Pandit and J. B. Joshi, "Mass and heat transfer characteristics of three phase sparged reactors," *Chemical Engineering Research and Design*, vol. 64, no. 2, pp. 125–157, 1986.

[17] S. Cohen and D. M. Marom, "Experimental and theoretical study of a rotating annular flow reactor," *The Chemical Engineering Journal*, vol. 27, no. 2, pp. 87–97, 1983.

[18] V. V. Ranade, J. B. Joshi, and A. G. Marathe, "Flow generated by pitched blade turbines II: simulation using k-e model," *Chemical Engineering Communications*, vol. 81, pp. 225–248, 1989.

[19] V. V. Ranade, J. R. Bourne, and J. B. Joshi, "Fluid mechanics and blending in agitated tanks," *Chemical Engineering Science*, vol. 46, no. 8, pp. 1883–1893, 1991.

[20] T. Ogihara, G. Matsuda, T. Yanagawa, N. Ogata, K. Fujita, and M. Nomura, "Continuous synthesis of monodispersed silica particles using Couette-Taylor vortex flow," *Journal of the Ceramic Society of Japan*, vol. 103, pp. 151–154, 1995.

[21] V. D. Mundale, H. S. Joglekar, A. Kalam, and J. B. Joshi, "Regeneration of spent activated carbon by wet air oxidation," *The Canadian Journal of Chemical Engineering*, vol. 69, no. 5, pp. 1149–1159, 1991.

[22] N. N. Gandhi, S. B. Sawant, and J. B. Joshi, "Specificity of a lipase in ester synthesis: effect of alcohol," *Biotechnology Progress*, vol. 11, no. 3, pp. 282–287, 1995.

[23] N. N. Gandhi, N. S. Patil, S. B. Sawant, J. B. Joshi, P. P. Wangikar, and D. Mukesh, "Lipase-catalyzed esterification," *Catalysis Reviews*, vol. 42, no. 4, pp. 439–480, 2000.

[24] A. B. Pandit and J. B. Joshi, "Hydrolysis of fatty oils: effect of cavitation," *Chemical Engineering Science*, vol. 48, no. 19, pp. 3440–3442, 1993.

[25] J. F. Birdwell Jr., J. McFarlane, R. D. Hunt et al., "Separation of ionic liquid dispersions in centrifugal solvent extraction contactors," *Separation Science and Technology*, vol. 41, no. 10, pp. 2205–2223, 2006.

[26] S. S. Deshmukh, S. Vedantam, J. B. Joshi, and S. B. Koganti, "Computational flow modeling and visualization in the annular region of annular centrifugal extractor," *Industrial & Engineering Chemistry Research*, vol. 46, no. 25, pp. 8343–8354, 2007.

[27] K. E. Wardle, T. R. Allen, M. H. Anderson, and R. E. Swaney, "Analysis of the effect of mixing vane geometry on the flow in an annular centrifugal contactor," *AIChE Journal*, vol. 55, no. 9, pp. 2244–2259, 2009.

[28] M. J. Sathe, S. S. Deshmukh, J. B. Joshi, and S. B. Koganti, "Computational fluid dynamics simulation and experimental investigation: study of two-phase liquid-liquid flow in a vertical Taylor-Couette contactor," *Industrial & Engineering Chemistry Research*, vol. 49, no. 1, pp. 14–28, 2010.

[29] R. J. Campero and R. D. Vigil, "Flow patterns in liquid−liquid Taylor−Couette−poiseuille flow," *Industrial & Engineering Chemistry Research*, vol. 38, no. 3, pp. 1094–1098, 1999.

[30] X. Zhu, R. J. Campero, and R. D. Vigil, "Axial mass transport in liquid-liquid Taylor-Couette-Poiseuille flow," *Chemical Engineering Science*, vol. 55, no. 21, pp. 5079–5087, 2000.

[31] T. Hong, L. S. Fan, and D. J. Lee, "Force variations on particle induced by bubble-particle collision," *International Journal of Multiphase Flow*, vol. 25, no. 3, pp. 477–500, 1999.

[32] Y. Li, G. Q. Yang, L. P. Zhang, and L. S. Fan, "Numerical studies of bubble formation dynamics in gas–liquid–solid fluidization at high pressures," *Powder Technology*, vol. 116, no. 2-3, pp. 246–260, 2001.

[33] Z. Cui and L. S. Fan, "Turbulence energy distributions in bubbling gas–liquid and gas–liquid–solid flow systems," *Chemical Engineering Science*, vol. 59, no. 8-9, pp. 1755–1766, 2004.

[34] W. Warsito and L. S. Fan, "Dynamics of spiral bubble plume motion in the entrance region of bubble columns and three-phase fluidized beds using 3D ECT," *Chemical Engineering Science*, vol. 60, no. 22, pp. 6073–6084, 2005.

[35] G. Q. Yang, D. Bing, and L. S. Fan, "Bubble formation and dynamics in gas–liquid–solid fluidization—a review," *Chemical Engineering Science*, vol. 62, no. 1-2, pp. 2–27, 2007.

[36] M. Van Sint Annaland, N. Deen, and J. A. M. Kuipers, "Numerical simulation of gas bubbles behaviour using a three-dimensional volume of fluid method," *Chemical Engineering Science*, vol. 60, no. 11, pp. 2999–3011, 2005.

[37] W. Dijkhuizen, I. Roghair, M. Van Sint Annaland, and J. A. M. Kuipers, "DNS of gas bubbles behaviour using an improved 3D front tracking model-Drag force on isolated bubbles and comparison with experiments," *Chemical Engineering Science*, vol. 65, no. 4, pp. 1415–1426, 2010.

[38] M. A. Van der Hoef, J. A. M. Kuipers, and J. Wang, "Coarse grid simulation of bed expansion characteristics of industrial-scale gas-solid bubbling fluidized beds," *Chemical Engineering Science*, vol. 65, no. 6, pp. 2125–2131, 2010.

[39] I. Roghair, Y. M. Lau, N. G. Deen et al., "On the drag force of bubbles in bubble swarms at intermediate and high Reynolds numbers," *Chemical Engineering Science*, vol. 66, no. 14, pp. 3204–3211, 2011.

[40] M. A. Van der Hoef, J. A. M. Kuipers, and J. Wang, "CFD study of the minimum bubbling velocity of Geldart A particles in gas-fluidized beds," *Chemical Engineering Science*, vol. 65, no. 12, pp. 3772–3785, 2011.

[41] D. Jain, N. G. Deen, J. A. M. Kuipers, S. Antonyuk, and S. Heinrich, "Direct numerical simulation of particle impact on thin liquid films using a combined volume of fluid and immersed boundary method ," *Chemical Engineering Science*, vol. 69, no. 1, pp. 530–540, 2012.

[42] R. A. Bakker and H. E. A. Van Den Akker, "A lagrangian description of micromixing in a stirred tank reactor using 1D-micromixing models in a CFD flow field," *Chemical Engineering Science*, vol. 51, no. 11, pp. 2643–2648, 1996.

[43] R. F. Mudde and H. E. A. Van Den Akker, "2D and 3D simulations of an internal airlift loop reactor on the basis of a two-fluid model," *Chemical Engineering Science*, vol. 56, no. 21-22, pp. 6351–6358, 2001.

[44] R. S. Oey, R. F. Mudde, L. M. Portela, and H. E. A. Van Den Akker, "Simulation of a slurry airlift using a two-fluid model," *Chemical Engineering Science*, vol. 56, no. 2, pp. 673–681, 2001.

[45] H. Hartmann, J. J. Derksen, C. Montavon, J. Pearson, I. S. Hamill, and H. E. A. van den Akker, "Assessment of large eddy and RANS stirred tank simulations by means of LDA," *Chemical Engineering Science*, vol. 59, no. 12, pp. 2419–2432, 2004.

[46] J. J. Derksen, K. Kontomaris, J. B. McLaughlin, and H. E. A. Van den Akker, "Large-eddy simulation of single-phase flow dynamics and mixing in an industrial crystallizer," *Chemical Engineering Research and Design*, vol. 85, no. 2, pp. 169–179, 2007.

[47] B. C. H. Venneker, J. J. Derksen, and H. E. A. Van den Akker, "Turbulent flow of shear-thinning liquids in stirred tanks—the effects of Reynolds number and flow index," *Chemical Engineering Research and Design*, vol. 88, no. 7, pp. 827–843, 2010.

[48] B. C. H. Venneker, J. J. Derksen, and H. E. A. Van den Akker, "Reply to comments on 'turbulent flow of shear-thinning liquids in stirred tanks—the effects of Reynolds number and flow index'," *Chemical Engineering Research and Design*, vol. 89, no. 10, pp. 2194–2195, 2011.

[49] V. V. Ranade and J. B. Joshi, "Flow generated by a disc turbine. I: experimental," *Chemical Engineering Research and Design*, vol. 68, no. 1, pp. 19–33, 1990.

[50] V. V. Ranade and J. B. Joshi, "Flow generated by a disc turbine. II: mathematical modelling and comparison with experimental data," *Chemical Engineering Research and Design*, vol. 68, no. 1, pp. 34–50, 1990.

[51] V. V. Ranade, V. P. Mishra, V. S. Saraph, G. B. Deshpande, and J. B. Joshi, "Comparison of axial flow impellers using a laser Doppler anemometer," *Industrial & Engineering Chemistry Research*, vol. 31, no. 10, pp. 2370–2379, 1992.

[52] A. W. Patwardhan and J. B. Joshi, "Design of gas-inducing reactors," *Industrial & Engineering Chemistry Research*, vol. 38, no. 1, pp. 49–80, 1999.

[53] A. W. Patwardhan and J. B. Joshi, "Relation between flow pattern and blending in stirred tanks," *Industrial & Engineering Chemistry Research*, vol. 38, no. 8, pp. 3131–3143, 1999.

[54] J. B. Joshi, "Computational flow modelling and design of bubble column reactors," *Chemical Engineering Science*, vol. 56, no. 21-22, pp. 5893–5933, 2001.

[55] M. R. Bhole, J. B. Joshi, and D. Ramkrishna, "CFD simulation of bubble columns incorporating population balance modeling," *Chemical Engineering Science*, vol. 63, no. 8, pp. 2267–2282, 2008.

[56] R. K. Reddy, J. B. Joshi, K. Nandkumar, and P. D. Minev, "Direct numerical simulations of a freely falling sphere using fictitious domain method: breaking of axisymmetric wake," *Chemical Engineering Science*, vol. 65, no. 6, pp. 2159–2171, 2010.

[57] T. V. Tamhane, J. B. Joshi, K. Mudali, R. Natarajan, and R. N. Patil, "Measurement of drop size characteristics in annular centrifugal extractors using phase Doppler particle analyzer (PDPA)," *Chemical Engineering Research and Design*, vol. 90, no. 8, pp. 985–997, 2012.

[58] J. B. Joshi and V. V. Ranade, "Computational fluid dynamics for designing process equipment: expectations, current status, and path forward," *Industrial & Engineering Chemistry Research*, vol. 42, no. 6, pp. 1115–1128, 2003.

[59] J. B. Joshi, "Gas phase dispersion in bubble columns," *The Chemical Engineering Journal*, vol. 24, no. 2, pp. 213–216, 1982.

[60] N. K. Nere, A. W. Patwardhan, and J. B. Joshi, "Liquid-phase mixing in stirred vessels: turbulent flow regime," *Industrial & Engineering Chemistry Research*, vol. 42, no. 12, pp. 2661–2698, 2003.

[61] T. Kumaresan and J. B. Joshi, "Effect of impeller design on the flow pattern and mixing in stirred tanks," *The Chemical Engineering Journal*, vol. 115, no. 3, pp. 173–193, 2006.

[62] A. K. Sahu, P. Kumar, A. W. Patwardhan, and J. B. Joshi, "CFD modelling and mixing in stirred tanks," *Chemical Engineering Science*, vol. 54, no. 13-14, pp. 2285–2293, 1999.

[63] M. W. Haque, K. D. P. Nigam, and J. B. Joshi, "Hydrodynamics and mixing in highly viscous pseudo-plastic non-newtonian solutions in bubble columns," *Chemical Engineering Science*, vol. 41, no. 9, pp. 2321–2331, 1986.

[64] J. B. Joshi, "Axial mixing in multiphase contactors—a unified correlation," *Chemical Engineering Research and Design*, vol. 58, pp. 155–165, 1980.

[65] K. Ekambara and J. B. Joshi, "Axial mixing in pipe flows: turbulent and transition regions," *Chemical Engineering Science*, vol. 58, no. 12, pp. 2715–2724, 2003.

[66] K. Ekambara and J. B. Joshi, "Axial mixing in laminar pipe flows," *Chemical Engineering Science*, vol. 59, no. 18, pp. 3929–3944, 2004.

[67] O. Lorenz, A. Schumpe, K. Ekambara, and J. B. Joshi, "Liquid phase axial mixing in bubble columns operated at high pressures," *Chemical Engineering Science*, vol. 60, no. 13, pp. 3573–3586, 2005.

[68] S. S. Thakre and J. B. Joshi, "CFD simulation of bubble column reactors: importance of drag force formulation," *Chemical Engineering Science*, vol. 54, no. 21, pp. 5055–5060, 1999.

[69] S. S. Gulawani, J. B. Joshi, M. S. Shah, C. S. RamaPrasad, and D. S. Shukla, "CFD analysis of flow pattern and heat transfer in direct contact steam condensation," *Chemical Engineering Science*, vol. 61, no. 16, pp. 5204–5220, 2006.

[70] C. S. Mathpati and J. B. Joshi, "Insight into theories of heat and mass transfer at the solid−fluid interface using direct numerical simulation and large eddy simulation," *Industrial & Engineering Chemistry Research*, vol. 46, no. 25, pp. 8525–8557, 2007.

[71] M. T. Dhotre and J. B. Joshi, "Two-dimensional CFD model for the prediction of flow pattern, pressure drop and heat transfer coefficient in bubble column reactors," *Chemical Engineering Research and Design*, vol. 82, no. 6, pp. 689–707, 2004.

[72] M. T. Dhotre, V. S. Vitankar, and J. B. Joshi, "CFD simulation of steady state heat transfer in bubble columns," *The Chemical Engineering Journal*, vol. 108, no. 1-2, pp. 117–125, 2005.

[73] S. S. Deshpande, C. S. Mathpati, S. S. Gulawani, J. B. Joshi, and V. R. Kumar, "Effect of flow structures on heat transfer in single and multiphase jet reactors," *Industrial & Engineering Chemistry Research*, vol. 48, no. 21, pp. 9428–9440, 2009.

[74] J. B. Joshi and M. M. Sharma, "Mass transfer and hydrodynamic characteristics of gas inducing type of agitated contactors," *The Canadian Journal of Chemical Engineering*, vol. 55, no. 6, pp. 683–695, 1977.

[75] B. N. Murthy, N. A. Deshmukh, A. W. Patwardhan, and J. B. Joshi, "Hollow self-inducing impellers: flow visualization and CFD simulation," *Chemical Engineering Science*, vol. 62, no. 14, pp. 3839–3848, 2007.

[76] B. N. Murthy, R. S. Ghadge, and J. B. Joshi, "CFD simulations of gas-liquid-solid stirred reactor: prediction of critical impeller speed for solid suspension," *Chemical Engineering Science*, vol. 62, no. 24, pp. 7184–7195, 2007.

[77] K. S. M. S. R. Rao, V. B. Rewatkar, and J. B. Joshi, "Critical impeller speed for solid suspension in mechanically agitated contactors," *AIChE Journal*, vol. 34, no. 8, pp. 1332–1340, 1988.

[78] V. B. Rewatkar, J. B. Joshi, and K. S. M. S. Raghava Rao, "Critical impeller speed for solid suspension in mechanically agitated three-phase reactors. 1. Experimental part," *Industrial & Engineering Chemistry Research*, vol. 30, no. 8, pp. 1770–1784, 1991.

[79] J. B. Joshi, S. B. Sawant, A. W. Patwardhan, D. J. Patil, S. S. Kshatriya, and N. K. Nere, "Relation between flow pattern and de-activation of enzymes in stirred reactors," *Chemical Engineering Science*, vol. 56, no. 2, pp. 443–452, 2001.

[80] E. L. Koschmieder, *Bénard Cells and Taylor Vortices*, Cambridge University Press, New York, NY, USA, 1993.

[81] M. Couette, "Études sur le frottement des liquides," *Annales de Chimie et de Physique 6*, vol. 21, pp. 433–510, 1890.

[82] A. Mallock, "Experiments on fluid viscosity," *Philosophical Transactions of the Royal Society A*, vol. 187, pp. 41–56, 1896.

[83] L. Rayleigh, "On the dynamics of revolving fluids," *Proceedings of the Royal Society of London A*, vol. 93, no. 648, pp. 148–154, 1916.

[84] G. I. Taylor, "Stability of a viscous liquid contained between two rotating cylinders," *Philosophical Transactions of the Royal Society A*, vol. 223, no. 605–615, pp. 289–343, 1923.

[85] H. Jeffreys, "Some cases of instability in fluid motion," *Proceedings of the Royal Society A*, vol. 118, no. 779, pp. 195–208, 1928.

[86] R. J. Donnelly, "Experiments on the stability of viscous flow between rotating cylinders. I. Torque measurements," *Proceedings of the Royal Society A*, vol. 246, no. 1246, pp. 312–325, 1958.

[87] S. Chandrasekhar, "The stability of spiral flow between rotating cylinders," *Proceedings of the Royal Society A*, vol. 265, no. 1321, pp. 188–197, 1962.

[88] A. Davey, "The growth of Taylor vortices in flow between rotating cylinders," *Journal of Fluid Mechanics*, vol. 14, pp. 336–368, 1962.

[89] P. H. Roberts, "Appendix. The solution of the characteristic valueproblems," *Proceedings of the Royal Society A*, vol. 283, p. 550, 1965.

[90] J. T. Stuart, "On the non-linear mechanics of hydrodynamic stability," *Journal of Fluid Mechanics*, vol. 4, pp. 1–21, 1958.

[91] D. J. Coles, "Transition in circular Couette flow," *Journal of Fluid Mechanics*, vol. 21, pp. 385–425, 1965.

[92] R. C. DiPrima and P. M. Eagles, "Amplification rates and torques for Taylor—vortex flows between rotating cylinders," *Physics of Fluids*, vol. 20, no. 2, pp. 171–175, 1977.

[93] J. E. Burkhalter and E. L. Koschmeider, "Steady supercritical Taylor vortex flow," *Journal of Fluid Mechanics*, vol. 58, pp. 547–560, 1973.

[94] C. D. Andereck, S. S. Liu, and H. L. Swinney, "Flow regimes in a circular Couette system with independently rotating cylinders," *Journal of Fluid Mechanics*, vol. 164, pp. 155–183, 1986.

[95] R. M. Lueptow, A. Docter, and K. Min, "Stability of axial flow in an annulus with a rotating inner cylinder," *Physics of Fluids A*, vol. 4, no. 11, pp. 2446–2455, 1992.

[96] M. J. Braun, R. K. Corder, and V. Kudriavtsev, "Flow visualization of the evolution of Taylor instabilities and comparison with numerical simulations," in *Proceedings of the ASME Pressure Vessels and Piping Conference (PVP '02)*, vol. 448-1 of *Computational Technologies for Fluid/Thermal/Structural/Chemical Systems With Industrial Applications*, pp. 45–54, August 2002.

[97] P. Desevaux, "Numerical flow visualization of the formation of Taylor cells in a laminar Taylor-Couette flow," *Journal of Visualization*, vol. 12, no. 2, pp. 91–92, 2009.

[98] E. Varechon, J. P. Prenel, and G. Cognet, "Visualization of Taylor cells formation," in *Proceedings of the 4th Triennial International Symposium on Fluid Control, Fluid Measurement, and Visualization (FLUCOME '94)*, pp. 577–582, Toulouse, France, 1994.

[99] K. M. Saqr, N. A. C. Sidik, H. S. Aly, and Y. A. ElDrainy, "Uncharacteristic phenomenon in the nonisothermal Taylor-Couette flow," in *Proceedings of the International Conference on Signal Processing Systems (ICSPS '09)*, pp. 879–883, Singapore, May 2009.

[100] E. Barnea and J. J. Mizrahi, "Separation mechanism of liquid-liquid dispersions in a deep later gravity settler: part I. The structure of the dispersion band," *Chemical Engineering Research and Design*, vol. 53, pp. 61–69, 1975.

[101] E. Barnea and J. J. Mizrahi, "Separation mechanism of liquid-liquid dispersions in a deep later gravity settler: part II. Flow patterns of the dispersed and continuous phases within the dispersion band," *Chemical Engineering Research and Design*, vol. 53, pp. 70–74, 1975.

[102] E. Barnea and J. J. Mizrahi, "Separation mechanism of liquid-liquid dispersions in a deep later gravity settler: part III. Hindered settling and drop to drop coalescence in the dispersion band," *Chemical Engineering Research and Design*, vol. 53, pp. 75–82, 1975.

[103] R. A. Leonard, "Solvent characterization using the dispersion number," *Separation Science and Technology*, vol. 30, no. 7–9, pp. 1103–1121, 1995.

[104] R. A. Leonard, "Recent advances in centrifugal contactor design," *Separation Science and Technology*, vol. 23, no. 12-13, pp. 1473–1487, 1988.

[105] T. V. Tamhane, J. B. Joshi, U. K. Mudali, R. Natarajan, and R. N. Patil, "Axial mixing in annular centrifugal extractors," *The Chemical Engineering Journal*. In press.

[106] V. V. Ranade, *Computational Flow Modelling For Chemical Reactor Engineering*, vol. 5, Academic Press, 2002.

[107] R. S. Leonard, R. H. Pelto, A. A. Ziegler, and G. J. Bernstein, "Flow over circular weirs in a centrifugal field," *The Canadian Journal of Chemical Engineering*, vol. 58, no. 4, pp. 531–534, 1980.

[108] V. V. Ranade and J. B. Joshi, "Flow generated by pitched blade turbines I: measurements using laser Doppler anemometer," *Chemical Engineering Communications*, vol. 81, no. 1, pp. 197–224, 1989.

[109] J. B. Joshi, N. K. Nere, C. V. Rane et al., "CFD simulation of stirred tanks: comparison of turbulence models. Part I: radial flow impellers," *The Canadian Journal of Chemical Engineering*, vol. 89, no. 1, pp. 23–82, 2011.

[110] J. B. Joshi, V. V. Ranade, S. D. Gharat, and S. S. Lele, "Sparged loop reactors," *The Canadian Journal of Chemical Engineering*, vol. 68, no. 5, pp. 705–741, 1990.

[111] J. Parker and P. Merati, "An investigation of turbulent Taylor-Couette flow using laser Doppler velocimetry in a refractive index matched facility," *Journal of Fluids Engineering*, vol. 118, no. 4, pp. 810–818, 1996.

[112] G. Baier, *Liquid-liquid extraction based on a new flow pattern: two-fluid Taylor-Couette flow [Ph.D. thesis]*, University of Wisconsin-Madison, Madison, Wis, USA, 2000.

[113] B. Haut, H. B. Amor, L. Coulon, A. Jacquet, and V. Halloin, "Hydrodynamics and mass transfer in a Couette-Taylor bioreactor for the culture of animal cells," *Chemical Engineering Science*, vol. 58, no. 3–6, pp. 777–784, 2003.

[114] K. Kataoka, H. Doi, T. Hongo, and M. Futagawa, "Ideal plug-flow properties of Taylor vortex flow," *Journal of Chemical Engineering of Japan*, vol. 8, no. 6, pp. 472–476, 1975.

[115] J. Legrand and F. Coeuret, "Circumferential mixing in one-phase and two-phase Taylor vortex flows," *Chemical Engineering Science*, vol. 41, no. 1, pp. 47–53, 1986.

[116] P. I. Pudijiono, N. S. Tavare, J. Garside, and K. D. P. Nigam, "Residence time distribution from a continuous Couette flow device," *The Chemical Engineering Journal*, vol. 42, no. 2, pp. 101–110, 1998.

[117] H. Desmet, G. V. Verelst, and G. V. Baron, "Local and global dispersion effects in Couette-Taylor flow—I. Description and modeling of the dispersion effects," *Chemical Engineering Science*, vol. 51, no. 8, pp. 1287–1298, 1996.

[118] H. Desmet, G. V. Verelst, and G. V. Baron, "Local and global dispersion effects in Couette-Taylor flow—II. Quantitative measurements and discussion of the reactor performance," *Chemical Engineering Science*, vol. 51, no. 8, pp. 1299–1309, 1996.

[119] S. S. Deshmukh, M. J. Sathe, and J. B. Joshi, "Residence time distribution and flow patterns in the single-phase annular region of annular centrifugal extractor," *Industrial & Engineering Chemistry Research*, vol. 48, no. 1, pp. 37–46, 2009.

[120] T. Kumaresan, N. K. Nere, and J. B. Joshi, "Effect of impeller design on the flow pattern and mixing in stirred tanks," *Industrial & Engineering Chemistry Research*, vol. 115, no. 3, pp. 173–193, 2006.

[121] X. Ni and C. C. Stevenson, "On the effect of gap size between baffle outer diameter and tube inner diameter on the mixing characteristics in an oscillatory-baffled column," *Journal of Chemical Technology & Biotechnology*, vol. 74, no. 6, pp. 587–593, 1999.

[122] B. B. Gupta, J. A. Howell, D. Wu, and R. W. Field, "A helical baffle for cross-flow microfiltration," *Journal of Membrane Science*, vol. 102, pp. 31–42, 1995.

[123] R. Deng, D. Y. Arifin, M. Y. Chyn, and C. H. Wang, "Taylor vortex flow in presence of internal baffles," *Chemical Engineering Science*, vol. 65, no. 16, pp. 4598–4605, 2010.

[124] O. Czarny, E. Serre, P. Bontoux, and R. M. Lueptow, "Interaction of wavy cylindrical Couette flow with endwalls," *Physics of Fluids*, vol. 16, no. 4, pp. 1140–1148, 2004.

[125] M. A. Sprague and P. D. Weidman, "Continuously tailored Taylor vortices," *Physics of Fluids*, vol. 21, no. 11, Article ID 009912PHF, pp. 1–8, 2009.

[126] R. Mullin and C. Bohm, "Bifurcation phenomena in a Taylor–Couette flow with asymmetric boundary conditions," *Physics of Fluids*, vol. 13, no. 1, p. 136, 2001.

[127] J. H. Kim and L. S. Kim, "Flow-accelerated corrosion behavior of SA106 Gr.C steel in alkaline solution characterized by rotating cylinder electrode," *Journal of the Korean Nuclear Society*, vol. 32, no. 6, p. 595, 2000.

[128] F. N. Shi and T. J. Napier-Munn, "Measuring the rheology of slurries using an on-line viscometer," *International Journal of Mineral Processing*, vol. 47, no. 3-4, pp. 153–176, 1996.

[129] J. H. Clark, *Chemistry of Waste Minimization*, Blackie, Academic and Professional Newyork, 1995.

[130] J. G. Sczechowski, C. A. Koval, and R. D. Noble, "A Taylor vortex reactor for heterogeneous photocatalysis," *Chemical Engineering Science*, vol. 50, no. 20, pp. 3163–3173, 1995.

[131] B. V. Loureiro, P. R. De Souza Mendes, and L. F. A. Azevedo, "Taylor-Couette instabilities in flows of Newtonian and power-law liquids in the presence of partial annulus obstruction," *Journal of Fluids Engineering*, vol. 128, no. 1, pp. 42–54, 2006.

[132] S. S. Deshmukh, J. B. Joshi, and S. B. Koganti, "Flow visualization and three-dimensional CFD simulation of the annular region of an annular centrifugal extractor," *Industrial & Engineering Chemistry Research*, vol. 47, no. 10, pp. 3677–3686, 2008.

[133] K. E. Wardle, T. R. Allen, and R. Swaney, "Computational fluid dynamics (CFD) study of the flow in an annular centrifugal contactor," *Separation Science and Technology*, vol. 41, no. 10, pp. 2225–2244, 2006.

[134] B. Wegner, A. Maltsev, C. Schneider, A. Sadiki, A. Dreizler, and J. Janicka, "Assessment of unsteady RANS in predicting swirl flow instability based on LES and experiments," *International Journal of Heat and Fluid Flow*, vol. 25, no. 3, pp. 528–536, 2004.

[135] G. Iaccarino, A. Ooi, P. A. Durbin, and M. Behnia, "Reynolds averaged simulation of unsteady separated flow," *International Journal of Heat and Fluid Flow*, vol. 24, no. 2, pp. 147–156, 2003.

[136] J. Rivalier, J. Duhamet, and F. Gandi, "Annular Centrifugal Extractor with Embedded Stirring Rotor," U.S. Patent 7, 134, 991, 2006.

[137] T. Watanabe, Y. Toya, and I. Nakamura, "Development of free surface flow between concentric cylinders with vertical axes," *Journal of Physics*, vol. 14, no. 1, pp. 9–19, 2005.

[138] A. Mahamdia, A. Bouabdallah, and S. E. Skali, "Effects of free surface and aspect ratio on the transition of the Taylor-Couette flow," *Comptes Rendus Mécanique*, vol. 331, no. 3, pp. 245–252, 2003.

[139] M. Ammar, B. Ahcène, and S. S. Eddine, "Écoulement de Taylor-Couette en géométrie finie et à surface libre," *The Canadian Journal of Chemical Engineering*, vol. 83, no. 4, pp. 652–657, 2005.

[140] N. Mujica and D. P. Lathrop, "Hysteretic gravity-wave bifurcation in a highly turbulent swirling flow," *Journal of Fluid Mechanics*, vol. 551, pp. 49–62, 2006.

[141] K. E. Wardle, T. R. Allen, M. H. Anderson, and R. E. Swaney, "Free surface flow in the mixing zone of an annular centrifugal contactor," *AIChE Journal*, vol. 54, no. 1, pp. 74–85, 2008.

[142] C. W. Hirt and B. D. Nichols, "Volume of fluid (VOF) method for the dynamics of free boundaries," *Journal of Computational Physics*, vol. 39, no. 1, pp. 201–225, 1981.

[143] K. E. Wardle, T. R. Allen, and R. Swaney, "CFD simulation of the separation zone of an annular centrifugal contactor," *Separation Science and Technology*, vol. 44, no. 3, pp. 517–542, 2009.

[144] K. E. Wardle, T. R. Allen, M. H. Anderson, and R. E. Swaney, "Experimental study of the hydraulic operation of an annular centrifugal contactor with various mixing vane geometries," *AIChE Journal*, vol. 56, no. 8, pp. 1960–1974, 2010.

[145] K. E. Wardle, "Open-source CFD simulations of liquid–liquid flow in the annular centrifugal contactor," *Separation Science and Technology*, vol. 46, no. 15, pp. 2409–2417, 2011.

[146] K. E. Wardle and T. Lee, "Finite element lattice Boltzmann simulations of free surface flow in a concentric cylinder," *Computers & Mathematics with Applications*. In press.

[147] J. Patra, J. B. Joshi, N. K. Pandey, U. K. Mudali, and R. Natarajan, *Chemical Engineering Communications*. In press.

[148] P. A. Haas, "Turbulent dispersion of aqueous drops in organic liquids," *AIChE Journal*, vol. 33, no. 6, pp. 987–995, 1987.

[149] E. Tison, "Caractérisation de la zone de mélange d'un extracteur centrifuge annulaire à effet Couette utilisé en extraction liquide-liquide," *[Ph.D. thesis]*, Institut National Polytechnique de Lorraine (INPL), 1996.

[150] K. E. Wardle and C. Pereira, "Advanced multi-fluid simulations and experiments of flow in liquid-liquid contactors," *Transactions of the American Nuclear Society*, vol. 104, p. 168, 2011.

[151] L. Štrubelj, I. Tiselj, and B. Mavko, "Simulations of free surface flows with implementation of surface tension and interface sharpening in the two-fluid model," *International Journal of Heat and Fluid Flow*, vol. 30, no. 4, pp. 741–750, 2009.

[152] G. Baier and M. D. Graham, "Two-fluid Taylor-Couette flow: experiments and linear theory for immiscible liquids between corotating cylinders," *Physics of Fluids*, vol. 10, no. 12, pp. 3045–3055, 1998.

[153] X. Zhu and R. D. Vigil, "Banded liquid-liquid Taylor-Couette-Poiseuille flow," *AIChE Journal*, vol. 47, no. 9, pp. 1932–1940, 2001.

[154] K. Atkhen, J. Fontaine, and J. E. Wesfreid, "Highly turbulent Couette-Taylor bubbly flow patterns," *Journal of Fluid Mechanics*, vol. 422, pp. 55–68, 2000.

[155] H. Djeridi, J. F. Fave, J. Y. Billard, and D. H. Fruman, "Bubble capture and migration in Couette-Taylor flow," *Experiments in Fluids*, vol. 26, no. 3, pp. 233–239, 1999.

[156] Y. Murai, H. Oiwa, and Y. Takeda, "Bubble behavior in a vertical Taylor-Couette flow," *Journal of Physics*, vol. 14, no. 1, pp. 143–156, 2005.

[157] Y. Shiomi, H. Kutsuna, K. Akagawa, and M. Ozawa, "Two-phase flow in an annulus with a rotating inner cylinder (flow pattern in bubbly flow region)," *Nuclear Engineering and Design*, vol. 141, no. 1-2, pp. 27–34, 1993.

[158] E. Magere, M. O. Deville, K. Atkhen, and J. Fontaine, " Simulation of the pressure distribution in a spent nuclear fuel reprocessing Taylor-Couette device," in *Proceedings of the 4th Eccomas Conference on Computational Fluid Dynamics*, vol. 1, p. 1094, Athens, Greece, September 1998.

[159] Y. Shiomi, S. Nakanishi, and H. Kutsuna, "CFD calculation for two-phase flow in concentric annulus with rotating inner cylinder," unpublished manuscript.

[160] W. M. J. Batten, S. R. Turnock, N. W. Bressloff, and S. M. Abu-Sharkh, "Turbulent Taylor-Couette vortex flow between large radius ratio concentric cylinders," *Experiments in Fluids*, vol. 36, no. 3, pp. 419–421, 2004.

[161] T. H. Van den Berg, S. Luther, D. Lathrop, and D. Lohse, "Drag reduction in bubbly Taylor-Couette turbulence," *Physical Review Letters*, vol. 94, Article ID 044501, 4 pages, 2005.

[162] K. Atkhen, *Etude Hydrodynamique D'un Extracteur Centrifgue Utilisant les Proprietes des Ecoulements de Couette-Taylor [Ph.D. thesis]*, University of Paris, 1998.

[163] R. A. Leonard, G. J. Bernstein, R. H. Pelto, and A. A. Ziegler, "Liquid-liquid dispersion in turbulent Couette flow," *AIChE Journal*, vol. 27, no. 3, pp. 495–503, 1981.

[164] R. Leonard, M. S. Regalbuto, S. Aase, H. Arafat, and J. Falkenberg, "Hydraulic performance of a 5-cm contactor for caustic-side solvent extraction," Tech. Rep. ANL-02/18, Argonne National Laboratory, 2002.

[165] A. Gandhir and K. E. Wardle, "CFD analysis of fluid flow above the upper weir of an annular centrifugal contactor," *Separation Science and Technology*, vol. 47, no. 1, pp. 1–10, 2012.

[166] N. T. Padial-Collins, D. Z. Zhang, Q. Zou, X. Ma, and W. B. VanderHeyden, "Centrifugal contactors: separation of an aqueous and an organic stream in the rotor zone (LA-UR-05-7800)," *Separation Science and Technology*, vol. 41, no. 6, pp. 1001–1023, 2006.

[167] J. F. Birdwell Jr. and K. K. Anderson, "Evaluation of 5-cm centrifugal contactor hydraulic and mass transfer performance for caustic-side solvent extraction of cesium," Tech. Rep. ORNL/TM-2001/137, Oak Ridge National Laboratory, 2001.

[168] J. Law, R. Tillotson, and T. Todd, "Evaluation of the hydraulic performance and mass transfer efficiency of the CSSX process with the optimized solvent in a single stage of 5.5-Cm diameter centrifugal Contactor," Tech. Rep. INEEL/EXT-02-01106, Idaho National Engineering and Environmental Laboratory, 2002.

[169] J. Law, D. Meikrantz, T. Garn, N. Mann, S. Herbst, and T. Todd, "Testing of commercially available engineering- and plant-scale annular centrifugal contactors for the processing of spent nuclear fuel," Tech. Rep. INL/CON-06-11498, Idaho National Laboratory, 2002.

[170] L. Wang, D. L. Marchisio, R. D. Vigil, and R. O. Fox, "CFD simulation of aggregation and breakage processes in laminar Taylor-Couette flow," *Journal of Colloid and Interface Science*, vol. 282, no. 2, pp. 380–396, 2005.

[171] J. B. Joshi and M. M. Sharma, "Liquid phase backmixing in sparged contactors," *The Canadian Journal of Chemical Engineering*, vol. 56, no. 1, pp. 116–119, 1978.

[172] J. B. Joshi and M. M. Sharma, "A circulation cell model for bubble columns," *Transactions of the Institution of Chemical Engineers*, vol. 57, pp. 244–251, 1979.

[173] A. A. Kulkarni, J. B. Joshi, V. Ravikumar, and B. D. Kulkarni, "Wavelet transform of velocity-time data for the analysis of turbulent structures in a bubble column," *Chemical Engineering Science*, vol. 56, no. 18, pp. 5305–5315, 2001.

[174] A. A. Kulkarni, J. B. Joshi, V. Ravikumar, and B. D. Kulkarni, "Identification of the principal time scales in the bubble column by wavelet analysis," *Chemical Engineering Science*, vol. 56, no. 20, pp. 5739–5747, 2001.

[175] J. B. Joshi, V. S. Vitankar, A. A. Kulkarni, M. T. Dhotre, and K. Ekambara, "Coherent flow structures in bubble column reactors," *Chemical Engineering Science*, vol. 57, no. 16, pp. 3157–3183, 2002.

[176] A. A. Kulkarni and J. B. Joshi, "Measurement of eddy diffusivity in bubble column and validation based on the intermittency models," *Chemical Engineering Science*, vol. 60, no. 22, pp. 6146–6159, 2005.

[177] A. V. Kulkarni and J. B. Joshi, "Estimation of hydrodynamic and heat transfer characteristics of bubble column by analysis of wall pressure measurements and CFD simulations," *Transactions of the Institution of Chemical Engineers*, vol. 84, pp. 601–609, 2006.

[178] M. V. Tabib and J. B. Joshi, "Analysis of dominant flow structures and their flow dynamics in chemical process equipment using snapshot proper orthogonal decomposition technique," *Chemical Engineering Science*, vol. 63, no. 14, pp. 3695–3715, 2008.

[179] S. S. Deshpande, J. B. Joshi, V. R. Kumar, and B. D. Kulkarni, "Identification and characterization of flow structures in chemical process equipment using multiresolution techniques," *Chemical Engineering Science*, vol. 63, no. 21, pp. 5330–5346, 2008.

[180] M. V. Tabib, M. J. Sathe, S. S. Deshpande, and J. B. Joshi, "A hybridized snapshot proper orthogonal decomposition-discrete wavelet transform technique for the analysis of flow structures and their time evolution," *Chemical Engineering Science*, vol. 64, no. 21, pp. 4319–4340, 2009.

[181] J. B. Joshi, M. V. Tabib, S. S. Deshpande, and C. S. Mathpati, "Dynamics of flow structures and transport phenomena, 1. Experimental and numerical techniques for identification and energy content of flow structures," *Industrial & Engineering Chemistry Research*, vol. 48, no. 17, pp. 8244–8284, 2009.

[182] C. S. Mathpatii, M. V. Tabib, S. S. Deshpande, and J. B. Joshi, "Dynamics of flow structures and transport phenomena, 2. Relationship with design objectives and design optimization," *Industrial & Engineering Chemistry Research*, vol. 48, no. 17, pp. 8285–8311, 2009.

[183] K. Ekambara, K. Nandakumar, and J. B. Joshi, "CFD simulation of bubble column reactor using population balance," *Industrial & Engineering Chemistry Research*, vol. 47, no. 21, pp. 8505–8516, 2008.

[184] M. R. Bhole, J. B. Joshi, and D. Ramkrishna, "Population balance modeling for bubble columns operating in the homogeneous regime," *AIChE Journal*, vol. 53, no. 3, pp. 579–588, 2007.

[185] L. L. Macaluso and D. H. Meikrantz, "Self-cleaning Rotor for a Centrifugal Separator," U.S. Patent 5, 908, 376, 1999.

[186] R. A. Leonard, "Design principles and applications of centrifugal contactors for solvent extraction," in *Ion Exchange and Solvent Extraction: A Series of Advances*, chapter 10, pp. 563–616, CRC Press, 2010.

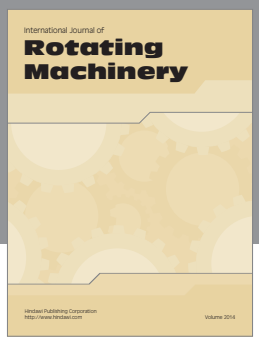

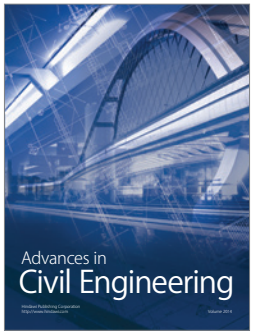

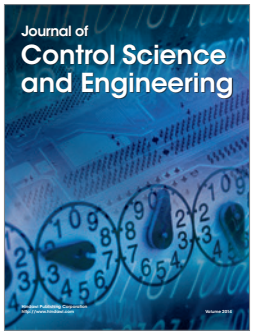

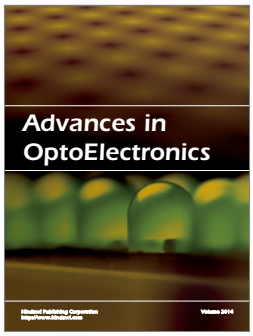

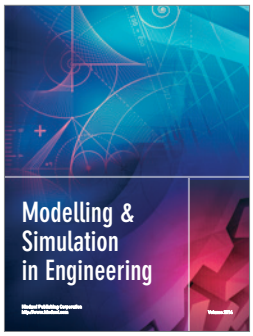

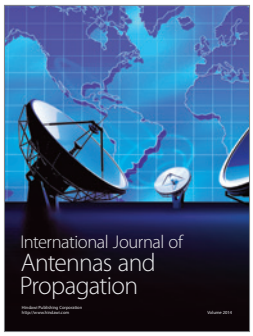

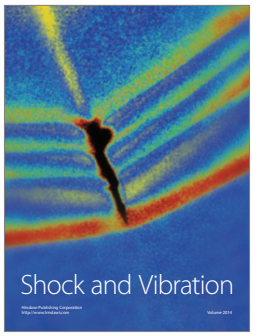

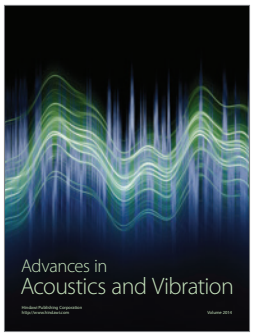

Hindawi

Submit your manuscripts at
http://www.hindawi.com